HIGHWAY RESEARCH RECORD

Number 249

Retaining Walls and Culverts

5 Reports

Subject Area	
23	Highway Drainage
27	Bridge Design
34	General Materials
62	Foundations (Soils)
63	Mechanics (Earth Mass)

HIGHWAY RESEARCH BOARD
DIVISION OF ENGINEERING NATIONAL RESEARCH COUNCIL
NATIONAL ACADEMY OF SCIENCES—NATIONAL ACADEMY OF ENGINEERING

Washington, D.C., 1968

Publication 1396

Price: $1.80

Available from

Highway Research Board
National Academy of Sciences
2101 Constitution Avenue
Washington, D.C. 20418

Department of Soils, Geology and Foundations

Eldon J. Yoder, Chairman
Purdue University, Lafayette, Indiana

Chester McDowell, Vice Chairman
Texas Highway Department, Austin

HIGHWAY RESEARCH BOARD STAFF

J. W. Guinnee

DIVISION B

Carl L. Monismith, Chairman
University of California, Berkeley

William P. Hofmann, Vice Chairman
New York Department of Transportation, Albany

COMMITTEE ON BURIED STRUCTURES
(As of December 31, 1967)

Reynold K. Watkins, Chairman
Utah State University, Logan

Jay R. Allgood
Bernard E. Butler
T. Y. Chu
T. F. deCapiteau
Ronald H. Drawsky
Kenneth S. Eff
L. H. Gabriel
Delon Hampton
D. A. Linger
Alex E. Mansour, Jr.
Ernest T. Selig
Harry H. Ulery
Howard L. White

COMMITTEE ON MECHANICS OF EARTH MASSES AND LAYERED SYSTEMS
(As of December 31, 1967)

Robert L. Schiffman, Chairman
University of Illinois, Chicago

Richard G. Ahlvin
William Baron
Donald M. Burmister
John T. Christian
Jacob Feld
A. A. Fungaroli
Delon Hampton
Milton E. Harr
R. L. Kondner
Raymond J. Krizek
Charles C. Ladd
Ulrich Luscher
Thurmul F. McMahon
Keshavan Nair
A. M. Richardson
Bruce B. Schimming
Werner E. Schmid
Frank H. Scrivner
Eugene L. Skok, Jr.
Robert D. Stoll
Aleksandar S. Vesic
Harvey E. Wahls
William G. Weber, Jr.
Russell A. Westmann

Department of Materials and Construction

R. L. Peyton, Chairman
State Highway Commission of Kansas, Topeka

HIGHWAY RESEARCH BOARD STAFF

R. E. Bollen and W. G. Gunderman

GENERAL MATERIALS DIVISION

John L. Beaton, Chairman
California Division of Highways, Sacramento

COMMITTEE ON CULVERTS AND CULVERT PIPE
(As of December 31, 1967)

Kenneth S. Eff, Chairman
Department of the Army, Washington, D. C.

Roger L. Brockenbrough
T. F. deCapiteau
W. B. Drake
C. J. Francis
C. Raymond Hanes
John G. Hendrickson, Jr.
L. R. Lawrence
Dwayne F. Nielson
Eric F. Nordlin
Robert A. Norton
Michael J. Sassani
Rockwell Smith
M. G. Spangler
Harold V. Swanson
J. E. Thompson
Adrianus Van Kampen
Reynold K. Watkins
Howard L. White

Contents

Foreword

Categorically the five papers in this RECORD are on soil-structure interaction. Soil pressures on buried structures are highly sensitive to both deformation of the structure and compression (and/or viscous flow) of the soil.

The paper by Allgood and Ciani concerns the structural performance of buried flexible cylinders as influenced by the soil modulus (compressibility) of the enveloping soil. Three papers report soil pressures on buried culverts. Davis and Bacher describe the methods for determining these pressures that are employed in California field tests. Linger and Fernandez have directed their study more specifically to the redistribution of pressure about buried structures depending upon the relative flexibility of the structure and the enveloping soil. The arching action of the soil causes major pressure redistribution. Pawsey and Brown report significant differences in soil pressures on buried structures caused by different methods of soil placement.

Schimming and Fischer propose a method for determining the optimum design of retaining walls. The method is based on model studies.

—Reynold K. Watkins

The Influence of Soil Modulus on the Behavior of Cylinders in Sand

J. R. ALLGOOD and J. B. CIANI, U. S. Naval Civil Engineering Laboratory, Port Hueneme, California

Experimental and theoretical results are given that provide information on the influence of soil properties on the behavior of buried cylinders whose axes are parallel to the surface. Sand type, density, and cylinder stiffness were varied in 12 static tests on 5-in. diameter thin metal cylinders. The stiffness of these cylinders was less than that of others in the literature for which complete information on soil properties was available.

This research provides a unified method for determining deflections and the critical buckling load based on the one-dimensional confined compression modulus from a standard laboratory test. Also, a relation for arching across buried cylinders that permits computation of the thrust at the haunches is given, and an equation is proposed for estimating interface pressure distribution from measurements of strains in the cylinder.

•THERE is doubt concerning the adequacy of currently employed methods for the design and analysis of horizontally oriented buried cylinders, particularly when the imposed loads are high. One reason for this doubt is that a rational way of relating the behavior of buried cylinders and standard soil properties determined in the laboratory is lacking. The prime objective of this research is to explore the problem area and to provide a unified methodology for defining behavior.

The stated goals were pursued through a series of experiments coupled with adaptation of the theory to a suitable form. In the limited test program, particular attention was paid to controlling and measuring soil properties and soil behavior.

The nature of the behavior of horizontally oriented buried cylinders of metal has been summarized by Meyerhof (1). Also, the potential modes of failure for thin metal cylinders have been described (2). Of the possible modes, those of prime practical concern are failure of the joints or the wall material due primarily to axial compression, collapse in the first symmetrical compression mode due to excessive horizontal expansion, and transitional (local) buckling due to insufficient cylinder and soil stiffness.

Regardless of the type of loading imposed on a buried cylinder, adequate rigidity must be provided and deflections must be limited to some preselected maximum. Once the failure criteria are established for a given installation, rational methods of design and analysis are needed that incorporate suitable material properties.

Useful relations between the modulus of elastic support, the effective modulus of elasticity, and the constrained soil modulus have been developed by Luscher (3). Coefficients from Luscher's equations are utilized here.

To facilitate design, Meyerhof proposed a deflection relation deduced from the Iowa formula and a crippling equation based upon plate buckling (1). In this paper a similar deflection relation is employed, a buckling equation for a cylinder in an elastic media is used, and an expression for the axial thrust based on an empirical relation for arching is developed.

Paper sponsored by Committee on Buried Structures and presented at the 47th Annual Meeting.

TABLE 1

TEST DESIGN

Parameters	Cylinder No.											
	21	22	23	24	25	26	27	28	29	30	31	32
Density γ, pcf	H 109.0	M 103.4	L 96.7	M 103.4	L 96.7	H 109.0	L 96.7	H 109.0	H 109.0	L 96.7	H 109.0	M 103.4
Angle of friction, φ	H[a]	H	H	H	L[b]	L	L	L	L	L	H	H
Thickness h, in.	M 0.012	H 0.018	H 0.018	M 0.012	L 0.006	L 0.006	H 0.018	L 0.006	M 0.012	L 0.006	M 0.012	H 0.018

Note: H, M, and L stand for high, medium, and low. [a]NCEL sand. [b]Beach sand.

A number of sources of cylinder test data are available (4, 5, 6, 3, 7, 8); however, much of the available information is for cylinders of relatively high stiffness. No results are available from thin cylinder tests in which the soil properties were well defined. The experiments described are intended to provide data in this regime for which information is lacking.

EXPERIMENTAL PROGRAM

Description of Experiment

Tests were performed on 12 cylinders consisting of 3 different thicknesses buried in 2 types of sand each at 3 different densities. The experiment (Table 1) was randomized, except that tests using one type of sand were performed in succession to keep the materials handling within practicable limits. Density and sand type were selected as variables because they are the primary soils parameters governing the soils modulus. Thickness was chosen because thickness and soils modulus are the prime parameters that control the buckling load.

All of the cylinders were 5 in. in inside diameter by 20 in. long and had thicknesses (Table 1) of 6, 12, and 18 mils. They were fabricated from C1010 steel, which had a yield strength of 89,000 psi and an ultimate strength of 99,000 psi. Depth of cover was 6 in. in all tests.

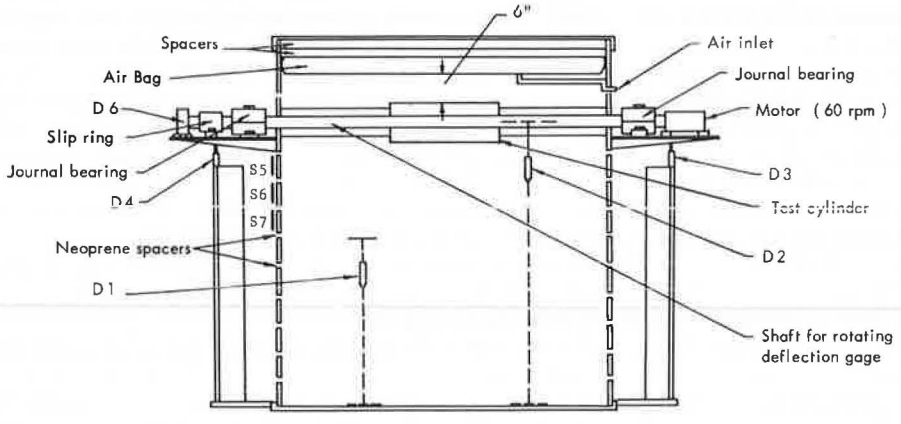

Figure 1. Section through segmented soil tank.

One of the sands employed was a sharp-grained material known as NCEL sand with a uniformity coefficient of 0.35; the other was a relatively round-grained beach sand with a uniformity coefficient of 0.75.

The tests were conducted in a segmented soil tank 5 ft in diameter constructed to minimize arching across the tank walls. In the tank, load is applied to a soil-structure specimen by pressurizing a pneumatic bag at the top surface of the soil. The bag reacts against a lid that, in turn, reacts against a closed frame around the tank.

A tubular opening passes diametrically through the soil tank (Fig. 1) to permit removal of a collapsible mandrel used to hold the cylinder to the proper shape and in the proper position during backfilling, and to accommodate a shaft that holds a rotating deflection gage. The shaft is attached to the ring immediately below the tubular opening; thus, the shaft moves downward as the soil is compressed. The tubular opening is formed by the test cylinder and two cantilevered pieces of pipe that are bolted to the rings at the elevation of the test cylinder.

Sand was placed in the tank by the sprinkling technique (4). Density was controlled by varying the flow rate and the height of drop. After the sand was filled to an elevation 1 in. above the invert and suitably leveled, a circular trough was cut in the sand to the dimensions of the cylinder with a special jig. The cylinder, containing the mandrel to retain a true circular shape, was then set in position and the backfill was placed. Ends of the mandrel were fastened to the cantilevered pipes to prevent movement of the cylinder during backfilling. After the backfilling was completed and the tank was closed, the collapsible mandrel was removed, the rotating deflection gage was installed, and the instrumentation was connected.

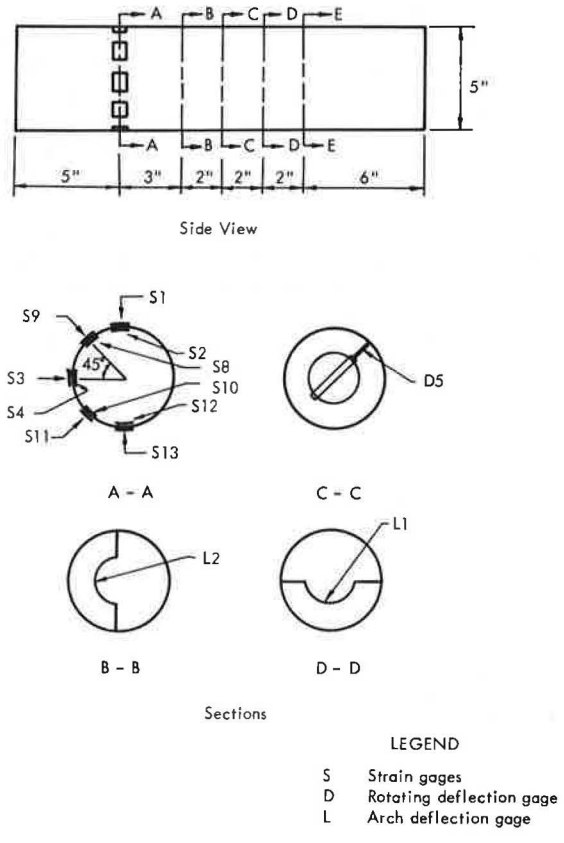

Figure 2. Instrumentation of steel cylinders.

Location and Purpose of Instruments

Location of the instrumentation, except for the pressure gages, is shown in Figures 1 and 2. Deflection gages D1 and D2 were differential transformers housed in pipes attached to the bottom of the tank. The cores were attached to disks that would deflect with the sand. These gages detected deflection relative to the bottom of the tank; the difference in their readings gave the average soil strain. Linear potentiometers D3 and D4 sensed deflection with respect to ground of the bearings of the rotating deflection gage, linear potentiometer D5. Gage D6 was a precision rotary potentiometer that gave the angular position of the rotating deflection gage.

Strain gages S5, S6, and S7, which measured hoop strain, were for purposes of determining the lateral deformation and stress of the soil. Strain gages S1 through S4 and S8 through S13 were for determining thrusts and moments. Strain gages S8 through S13 were included only on a few of the cylinders to provide supplementary information for interface pressure computations. The loop gages were to provide backup and check deflection measurements.

Surface pressure was applied in increments and records were taken

at each increment. The recorded data were subsequently punched on IBM cards and processed with the assistance of a digital computer.

RESULTS OF EXPERIMENTS

Test Results

Soil Properties—Initial densities determined by the sand replacement method are given in Table 1. Vane shear measurements also were made to supplement the density measurements and to provide information on the variation of shear resistance with depth. These measurements showed that the vane shear resistance increases relatively uniformly with depth and that the shear resistance increases markedly with increase in density as would be expected.

A study of the dependence of the coefficient of lateral earth pressure, K_o, on density and type of sand showed that above about 10 psi, there was very little change in the computed values of K_o with load or depth. Further, at depths of 10 in. or more there was only a small difference in K_o values for the two types of sands used. Average values were 0.45 for the NCEL sand and 0.48 for the beach sand. Stress-strain curves, based on the average strain between gages D1 and D2 were obtained for each setup (Fig. 3).

Deflections—In interpreting the behavior of the cylinders, it is well to remember that circumferential waves may develop around the perimeter of low stiffness buried cylinders at relatively small loads. The circumferential waves are superimposed on the fundamental elliptical-shaped deflection pattern. This behavior was first demonstrated by Bulson (9). Plots of load versus horizontal expansion of cylinders buried in granular materials tend to have the same shape as the stress-strain diagram of the soil, as may be seen by comparing the soil stress-strain curves (Fig. 3) and the corresponding load-deflection plots (Figs. 4 and 5). The load-deflection relation would be expected to be linear only if the modulus of elasticity of the soil remains constant. As is readily observed from the soil stress-strain diagrams (Fig. 3), for the tests reported here, the modulus varies with load; consequently, it is necessary to use a modulus in load-deflection relations such as the Iowa formula corresponding to the peak pressure producing the deflection of interest. A basic fault of the Iowa formula has been that the modulus used in the original formula was not related to any standard soil property readily measured in the laboratory. One of the aims of the reported research was to correct this deficiency.

Deflections of the cylinders depend primarily on the applied pressure and the modulus of the soil, as indicated by the Iowa formula. A heuristic development of the Iowa formula is readily achieved by considering the right (or left) one-half of the cylinder as an equivalent plate deflecting into the soil. In Figure 6, the average horizontal displacement may be expressed as $(C_1 \Delta x/2)$, and the effective width of the plate may be

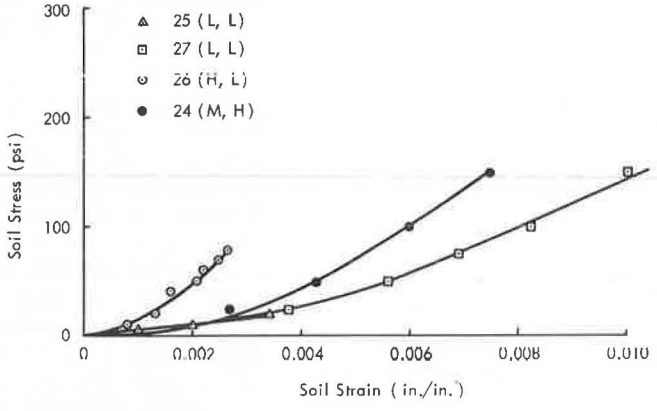

Figure 3. Soil stress-strain curves.

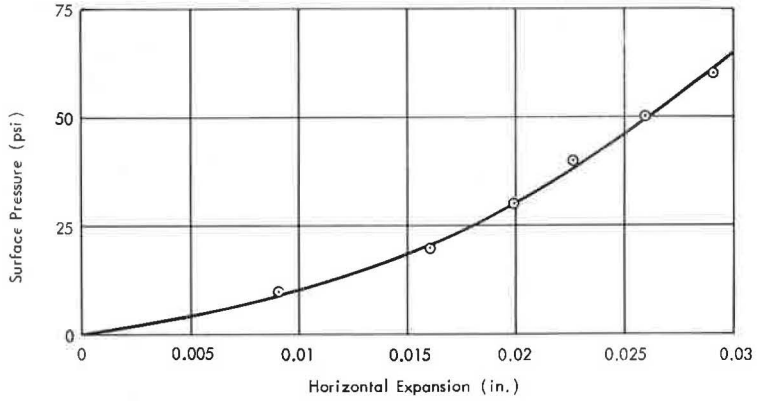

Figure 4. Load deflection curve, test 26.

taken as C_2D. The stress developed at the interface of the soil and the plate is C_3K_0p, where K_0 is the coefficient of lateral earth pressure. Assuming that the shape factor needed to account for the length-width ratio is one (a satisfactory assumption for granular soils), the effective soil modulus may be expressed as

$$E_S = \frac{C_3K_0p}{(C_1\Delta x/2)/C_2D} \tag{1}$$

where p is the surface pressure. This may be written as

$$\frac{\Delta x}{D} = 2\frac{C_2C_3}{C_1}K_0\frac{p}{E_S} \tag{2}$$

which is the recognizable form of the Iowa formula for thin-walled cylinders.

Luscher (3) has shown that the modulus for elastic systems is related to the confined compression modulus, M_C, by the relation

$$E_S = C_4M_C \tag{3}$$

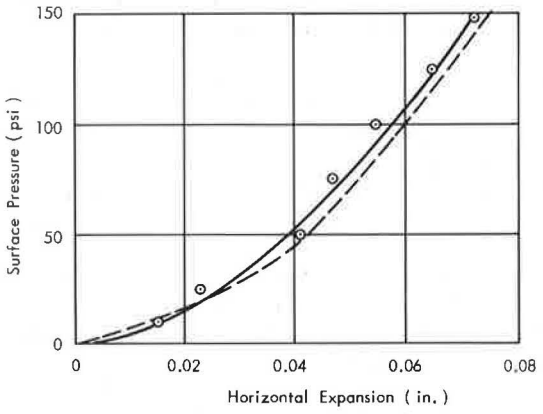

Figure 5. Load deflection curve, test 24.

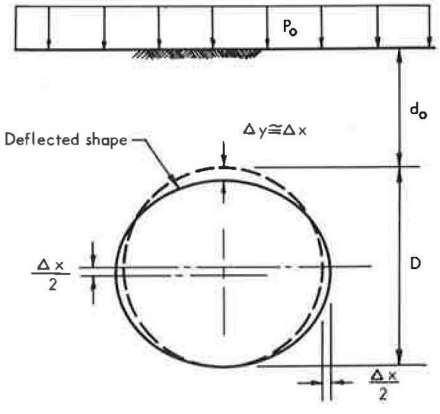

Figure 6. Deflected shape of cylinder.

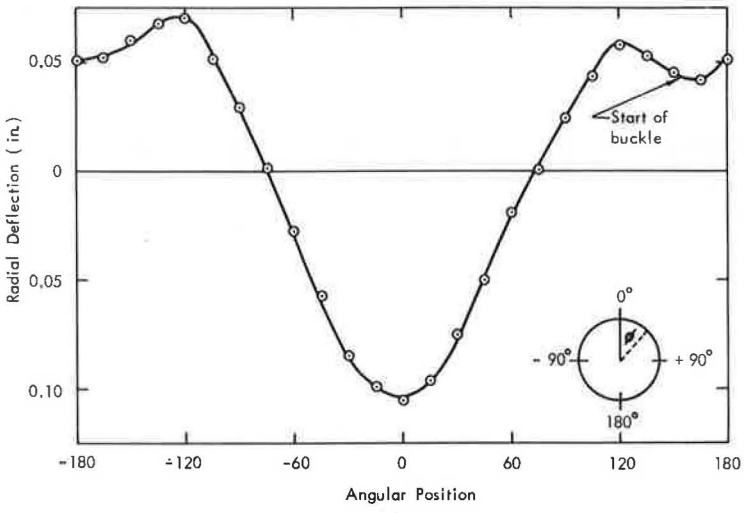

Figure 7. Deflection curve, test 24 at 100 psi.

where C_4 is a constant (0.577 for large soil thickness to diameter ratios). Substituting the latter relation in Eq. 2 gives

$$\frac{\Delta x}{D} = 2 \frac{C_2 C_3}{C_1 C_4} K_o \frac{p}{M_c} \tag{4}$$

Back calculating the quantity $C_5 = C_2 C_3 K_o / C_1 C_4$ from the test data gives a value of 1.0 ±15 percent. Therefore

$$\frac{\Delta x}{D} = 2.0 \frac{p}{M_c} \tag{5a}$$

Eq. 4 reduces to the easily rememberd relation

$$\frac{\Delta x}{D} = 2\epsilon \tag{5b}$$

where ϵ is the soil strain. Eq. 5 is compared with the test data for test 24 in Figure 5; it fits the test data well if M_c or ϵ is taken at the pressure for which the deflection is to be determined.

The test results show that the plots of surface pressure versus horizontal expansion for tests at a given density level are nearly the same. Differences in magnitude of the deflection within each of the three groupings are readily accounted for by differences in stiffness as indicated by the vane shear resistance.

A typical deflected shape of a test cylinder is shown in Figure 7. The localized inward deflection at 170 deg near the bottom of the cylinder is the beginning of an inward buckle.

Strains—Thrust and Moment—In all tests the strains remained elastic up to the time of failure, and in most cases, the strains at the sides increased approximately linearly with load. Regression analyses with strain as the dependent variable and density, angle of friction of the sand, cylinder thickness, and surface pressure as independent variables were run using strain on the extrados at the sides, strain on the intrados at the sides, and the difference and sum of the strains on the extrados and intrados at the

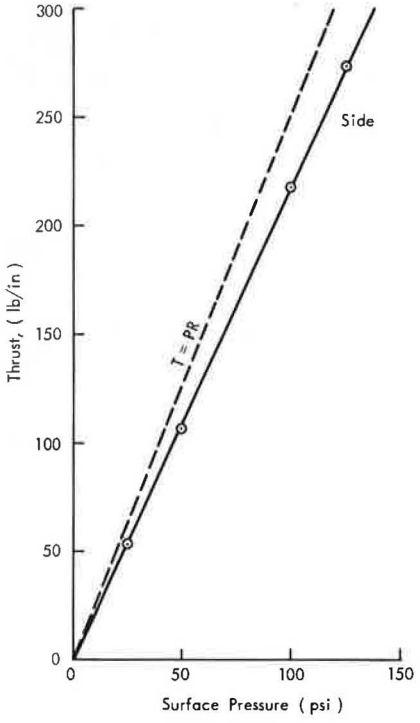

Figure 8. Thrust, test 24.

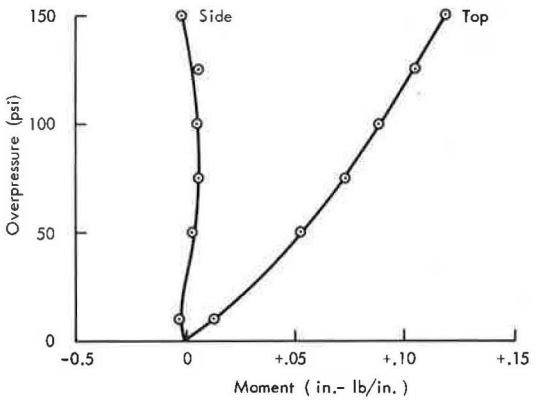

Figure 9. Moments in cylinder, test 24.

sides. The results show that sand type has very little effect on the strains induced at the springing (side) of a buried cylinder.

Thrusts and moments induced in the cylinder walls were determined from the strain readings. A plot of thrust as a function of load for test 24 is shown in Figure 8. Most of the thrust-load plots were straight lines through zero; however, a few were offset from zero. The variation of moment with load at the top and side for test 24 is shown in Figure 9. As would be expected, there was a wide variation in induced moments among the test cylinders; however, the moments in all cylinders remained less than the yield moment of the section in simple bending. They were, in most cases, considerably less than corresponding moments from the elastic theory.

Arching—The thrusts at the sides of the cylinder were utilized to determine the arching across the cylinder. In this instance, arching is defined as the shear in the soil on the vertical planes through the extreme sides of the cylinder; it equals the surface pressure times the radius minus the thrust at the side of the cylinder. The amount of load assumed by the soil is indicated by the vertical distance between the solid and dashed lines in Figure 8, where the dashed line represents the product of the surface pressure times the cylinder radius.

Arching over any given cylinder is seen to be essentially a constant percentage of the surface pressure (Table 2). Analysis of the data indicates that there is also a relatively small dependence of arching on density. Arching for the systems at high initial

TABLE 2

ARCHING OVER CYLINDERS

Test No.	Experiment Design Conditions	Arching (%)	Test No.	Experiment Design Conditions	Arching (%)
21	HHM	28	27	LLH	15
22	MHH	3	28	HLL	40
23	LHH	0	29	HLM	26
24	MHM	13	30	LLL	18
25	LLL	10	31	HHM	38
26	HLL	26	32	MHH	33

density averaged 32 percent with a variation from 26 to 40 percent. Arching for the systems at medium and low density averaged 9 percent with a variation from 0 to 18 percent. The reason for the discrepancy among tests at a given density level appears to lie mainly in imperfect seating of the cylinder during construction of the structure-sand system.

An insight into the nature of arching in densely compacted sands can be obtained from the empirical Gill-True arching equation (10), which may be expressed as

$$1 - \frac{A}{A_o} = e^{-n\varphi} \tag{6}$$

where

$$\varphi = A_g \frac{M_c}{p_i} \zeta \tag{6a}$$

$$A_g = \frac{Sd_o}{A_s D} \tag{6b}$$

and where

A = percent arching over structure;
A_o = maximum arching, %;
n = empirically determined constant;
A_g = geometry factor;
M_c = one-dimensional compression secant modulus;
p_i = interface pressure;
ζ = relative deflection between soil and structure;
S = plan perimeter of structure;
d_o = depth of cover;
A_s = plan area of structure; and
D = width of structure (cylinder diameter).

This empirical relation has been found to fit all available pertinent arching data.

Eq. 6 can be solved for A if suitable expressions for p_i and ζ can be developed. The average interface pressure may be expressed as

$$p_i = (1 - A)\, p_o \tag{7}$$

From Figure 6, the average relative deflection between the soil over the cylinder and that in the adjacent free field is

$$\zeta \cong \frac{1}{2}\left(\Delta x + \frac{\Delta x}{2}\right) = \frac{3}{4}\,\Delta x \tag{8}$$

Δx is determinable from Eq. 5. Substituting Eq. 5 in Eq. 8 and Eqs. 7 and 8 in Eq. 6 gives

$$1 - \frac{A}{A_o} = e^{-1.5n \frac{A_g D}{1 - A}} \tag{9}$$

For structures of rectangular plan, such as horizontally oriented cylinders, A_g may be expressed as

$$A_g = \frac{2d_o}{D^2}\left(1 + \frac{D}{L}\right) \tag{10}$$

where L = length of structure.

Substituting this relation in Eq. 9 and solving the resulting expression to get the arching terms on the left gives

$$\left(1 - \frac{A}{A_o}\right)^{1 - A} = e^{-3n\frac{d_o}{D}\left(1 + \frac{D}{L}\right)} \tag{11}$$

Eq. 11 with $A_o = 0.87$ and $n = 0.135$, as determined for a sharp-grained sand, gives $A = 37$ percent, as compared to an average arching of 32 percent determined from the experiment for the cylinders in dense sand.

For long cylinders, Eq. 11 indicates that the amount of arching is solely dependent on the depth of cover to diameter ratio. Analysis of the data shows a dependence on density not evidenced in Eq. 11; however, this expression appears to approximate arching correctly for dense backfills.

Since arching can be determined from Eq. 11, the induced thrust can be calculated from

$$N = (1 - A)(p_o r + \gamma d_o) \tag{12}$$

where γ = density. One might ask whether or not arching causes reductions in the horizontal expansion and the critical buckling load. For practical purposes the answer is no. The amount of arching over a thin metal cylinder subjected to a uniform surface pressure has no influence on deflection or the buckling load. The reason is that, as shown by Eqs. 5 and 16, the deflection and the buckling load depend primarily on the soil stiffness and not on the induced thrust. It is, of course, important to know the thrust for designing joints and insuring against unwanted compression yielding.

Interface Pressures—For thin cylinders it is theoretically possible to determine the interface pressure from measurements of strain. One approach is to use strain measurements to determine the radius of curvature and then to utilize the fact that for cylinders of small stiffness the interface pressure is equal to the thrust divided by the radius of curvature. From the theory of plates and shells the unit strain due to bending is

$$\epsilon = -\frac{c}{1 - \frac{c}{r}}\left(\frac{1}{\rho} - \frac{1}{r}\right) \tag{13}$$

where

ϵ = unit strain in outer fiber due to bending,
r = original radius of curvature,
ρ = deformed radius of curvature, and
c = distance from neutral axis to extreme outer fiber.

Solving for the deformed radius of curvature gives the expression

$$\rho = \frac{1}{\frac{1}{r} - \frac{\epsilon}{c}\left(1 - \frac{c}{r}\right)} \tag{14}$$

The term c/r is negligible compared to 1 for thin cylinders. Since the thrust is readily determined from strain measurements, for cylinders where the bending resistance is small the interface pressure may be expressed as

$$p_i \cong \frac{N}{\rho} \tag{15}$$

Alternately, the matrix theory of structural analysis may be employed to find the interface pressures from moments and thrusts computed from strain measurements.

TABLE 3

INTERFACE PRESSURE

Cylinder No.	Surface Pressure (psi)	Interface Pressure			
		Top		Side	
		p	p′	p	p′
31	10	7.3	7.2	3.6	4.8
	50	32.0	32.5	20.0	24.6
	100	61.6	61.8	40.9	48.9
32	10	5.0	5.5	5.3	4.8
	50	25.8	31.4	28.1	24.7
	100	53.1[a]	71.5	56.0[a]	49.8

[a]Values are low because of development of circumferential waves.

p = nodal pressure determined by matrix method using thrust and moments as input.
p′ = interface pressure determined from radius of curvature and thrust, p = N/ρ.

The methodology and a computer code for accomplishing this have been developed (12). A comparison between the interface pressure determined from the two methods just outlined gives reasonable agreement (Table 3), except at high loads when circumferential waves develop. The computer analysis shows that large interface shears develop and that the normal pressure distribution is fairly uniform, except that it is lower in the top and bottom regions than on the sides. It is worth noting that both methods may be used for determining the interface pressure distribution on a thin buried cylinder at specified times during a dynamic test. This is possible since the inertia of thin cylinders will be very small compared to the inertia of the confining soil mass.

Bottom view

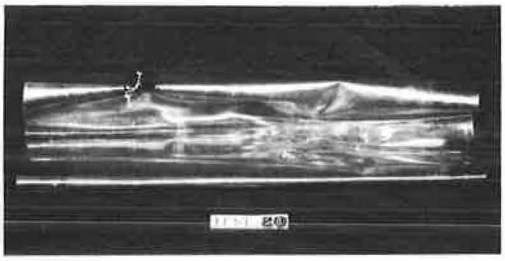

Bottom view

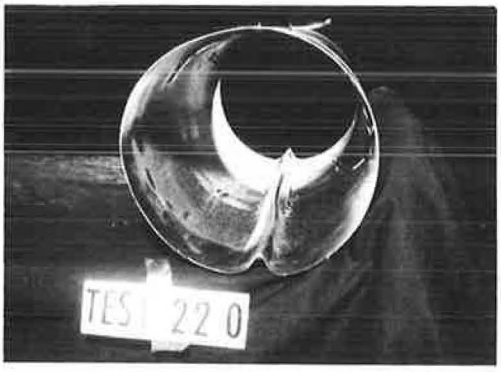

End view

Figure 10. Buckled cylinder, test 22.

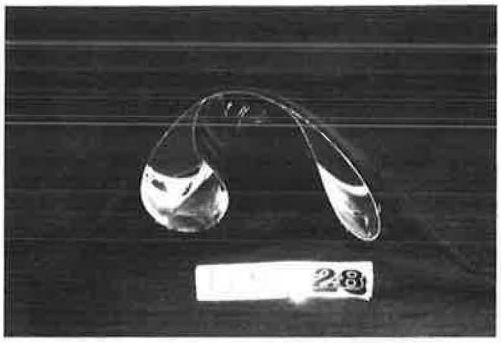

End view

Figure 11. Buckled cylinder, test 28.

TABLE 4
FAILURE LOADS

Cylinder No.	Experimental p	Buckling Load (psi) Interface p (1-A) p_{cr}	Theoretical 0.433p	Theoretical 0.612p
21	220	170[a]	90.7	128.2
22	237	180	145.7	205.8
23	247	178	165.7	234.2
24	266	246	98.9	139.7
25	75	51	18.5	26.1
26	123	81	40.1	56.6
27	247	218	147.1	207.9
28	121	75	39.7	56.1
29	300	210[a]	144.4	204.1
30	73	59	21.6	30.6
31	250	159	101.0	142.7
32	150	191[b]	155.0	219.0

[a]Not loaded to failure. [b]Estimated from test 22.

Buckling—Typical buckling failures for cylinders with high and low thicknesses are shown in Figures 10 and 11, respectively. Failures got progressively more severe until for the thinnest cylinder, test 28, there occurred essentially a complete collapse.

Critical buckling loads of the test cylinders and corresponding values from the Chelapati theory (11) are given in Table 4. For large length to radii ratios, large radii to thickness ratios, and large values of the so-called foundation coefficient (conditions applicable in the tests), the Chelapati theory may be expressed in explicit form for the case of all-around soil support as

$$p_{cr} = 0.612\sqrt{\frac{E_s E}{(r/t)^3}} \tag{16}$$

and for the case of soil support only on the outward deflecting lobes of the circumferential waves as

$$p_{cr} = 0.433\sqrt{\frac{E_s E}{(r/t)^3}} \tag{17}$$

where

p_{cr} = critical buckling pressure,
t = cylinder thickness,
r = cylinder radius,
E = modulus of the cylinder material, and
E_s = modulus of the soil = 0.577 M_c.

These relations are applicable where the depth of cover equals one diameter or greater. As in the modified deflection relation, the soil modulus in these equations must be taken at the failure load. Since the failure load is not usually known, an iteration process may be necessary to arrive at the correct buckling load.

The buckling data indicate that for very thin cylinders where circumferential waves are likely to develop Eq. 17 should be used. For values of the foundation coefficient greater than 5,000, it should be sufficient to use the relation for all-around support.

Other Considerations—There has been some question in the past about whether or not the effective properties of the soil surrounding a buried cylinder should be represented

as a hexagonally cross-anisotropic or other idealized material with different properties in the different principal directions.

Results of the present research indicate that for structural design purposes, the modulus is the only soil property required, assuming that there are no water problems. The reason is that there is a small variation in K_0 for densely compacted granular backfill materials; consequently, K_0 does not enter the deflection or buckling equations.

Of course, near the surface boundary the soil modulus, the coefficient of lateral earth pressure, and other soil properties and indexes of soil properties decrease rapidly. Thus, for shallow depths of cover, crown deflections would be expected to be larger and critical buckling loads would be expected to be smaller than those indicated by Eqs. 16 and 17. Complete documentation of the experiments outlined may be found elsewhere (12).

CONCLUSIONS

From the experimental results and the coupled analytical investigations, it is concluded that:

1. Sand type has little effect on the strains induced in a cylinder by the surface load.
2. The coefficient of lateral earth pressure varies only slightly for surface loads greater than 10 psi and is not greatly different for the sharp-grained or round-grained dry sands.
3. For the static design of buried thin metal cylinders, critical load and deflection relations employing only one soil parameter are adequate. (a) The pertinent modulus may be determined from the confined one-dimensional stress-strain curve of the soil. (b) The soil modulus used must correspond to the one-dimensional compression secant modulus at the surface pressure of interest.
4. Deflections of thin buried cylinders corresponding to a given loading are governed by the soil modulus, which is primarily dependent upon the initial density of the soil. Vane shear strength is a good index of the initial density.
5. Interface soil pressures can be determined from measurements of strain in the cylinder.
6. Critical buckling loads may be determined from the Chelapati theory. For very thin-walled cylinders, the buckling load should be based on the relations for support on the outward acting lobes of the circumferential waves only.

Relations for determining deflection, buckling, arching, and induced thrust are given—all of which are dependent upon only one easily determined soil property, the one-dimensional confined compression modulus. These conclusions are limited to the conditions and configuration of the research presented.

REFERENCES

1. Meyerhof, G. G. Composite Design of Shallow-Buried Steel Structures. Paper presented at the Annual Conference of the Canadian Good Roads Association, Halifax, N. S., Sept. 8, 1966. Copies available from Corrugated Metal Pipe Institute, Suite 207, Crestview Plaza, Port Credit, Ontario.
2. Allgood, J. R. The Behavior of Shallow-Buried Cylinders. Proc. Symposium on Soil-Structure Interaction, University of Arizona, Tucson, Sept. 1964.
3. Luscher, U. Buckling of Soil-Surrounded Tubes. Jour. Soil Mech. and Foundations Div., ASCE, Vol. 92, No. SM6, Proc. Paper 4990, Nov. 1966.
4. Doris, A. F. Response of Horizontally Oriented Buried Cylinders to Static and Dynamic Loading. U.S. Army Engineer Waterways Experiment Station, TR-1-682, Vicksburg, Miss., July 1965.
5. Hoeg, K. Pressure Distribution on Underground Structural Cylinders. Air Force Weapons Laboratory, TR-65-98, Contract AF 29(601)-6368 with Massachusetts Institute of Technology, Kirtland Air Force Base, New Mexico, April 1966.

6. Donnellan, B. A. The Response of Buried Cylinders to Quasi-Static Overpressures. Air Force Weapons Laboratory, WL TDR-64-13, Contract AF 29(601)-6002 with the University of New Mexico, Kirtland Air Force Base, New Mexico, Sept. 1964.
7. Whitman, R. V., and Luscher, U. Basic Experiment into Soil-Structure Interaction. Jour. Soil Mech. and Foundations Div., ASCE, Vol. 88, No. SM6, Proc. Paper 3366, Dec. 1962.
8. Marino, R. L., Jr. A Study of Static and Dynamic Resistance of Structural Elements. Air Force Weapons Laboratory, WL TR-64-122, Contract AF 29(601)-5372 with IIT Research Institute, Kirtland Air Force Base, New Mexico, July 1965.
9. Bulson, P. S. Deflection and Collapse of Buried Tubes. Military Engineering Experimental Establishment, Rept. RES 7/1, Christchurch, Hampshire, England, Nov. 1962.
10. Gill, H. L., and True, D. G. Active Arching of Sand During Static Loading. U.S. Naval Civil Engineering Laboratory, TN-759, Port Hueneme, California, Nov. 1965.
11. Chelapati, C. V. Critical Pressures for Radially Supported Cylinders. U. S. Naval Civil Engineering Laboratory, TN-773, Port Hueneme, California, Jan. 1966.
12. Allgood, J. R., Ciani, J. B., and Lew, T. The Influence of Soil Modulus on the Behavior of Cylinders in Sand. U.S. Naval Civil Engineering Laboratory Report, Port Hueneme, California, in publication.

California's Culvert Research Program—Description, Current Status, and Observed Peripheral Pressures

RAYMOND E. DAVIS and ALFRED E. BACHER, California Division of Highways

The California Division of Highways is performing an extensive research program to determine structural behavior of buried conduits. Field studies include observations of three arch culverts, two rigid concrete pipes, and two flexible (structural plate) pipes. Measurements include peripheral and embankment pressures, internal strains, and displacement fields. Parameters include Method B (imperfect ditch) and Method A (positive projection) backfill; well graded and poorly graded structure backfill; and, for the pipes, numerous bedding conditions.

Theoretical studies include a finite element analysis of embankment pressures, taking into account sequence of construction operations and the baled straw layers; and neutral point analyses of arch culvert behavior.

A quasi-theoretical method of inferring soil pressures from a culvert's displacement field has been developed. Model studies for verification are planned.

•THIS paper provides an overall description of the culvert research program and is a preliminary publication of some observed peripheral effective densities acting at the soil structure interfaces and in the embankments.

SCOPE

The program has elicited sufficient interest on the part of various individuals and organizations to warrant publication of a brief resumé describing the nature of the work and some of the results which have been obtained to date. In general, discussion of results is limited to plots of peripheral pressures observed for those prototype culverts for which the work is sufficiently far advanced. Only limited conclusions are offered.

DESCRIPTION OF RESEARCH PROGRAM

The various phases of the project are briefly summarized in Table 1.

RESULTS OBSERVED TO DATE

Arch Culvert Research

Phase 1—San Luis Reservoir—One result of the project was the development of a computerized analysis of arch culvert behavior based on the "neutral point" method (1, 2). The program determines bending moments, thrusts, and shears and resulting internal stresses for individual voussoir loads or assumed hydrostatic loadings. It also takes into account the effects of soil friction acting along the extrados, and differential footing movements. The program is written in FORTRAN IV (E level) for an IBM System/360.

Paper sponsored by Committee on Buried Structures.

TABLE 1

SUMMARY OF CULVERT RESEARCH

Phase	Cost ($000)	Parametric Conditions			Parameters Measured
		Bedding	Backfill	Structural Section	
Completed Projects:					
San Luis Reservoir 10-ft RC arch, 200-ft rock fill, broad canyon	86	Bedrock and embankment	Method B (2 types)	Special	Peripheral pressures Internal strains Internal stresses Displacements Embankment pressures Embankment settlements
Current Projects:					
Posey Canyon 8-ft RC arch, 240-ft fill, V canyon	102	Bedrock	Method A & Method B (3 types)	Standard & special	Peripheral pressures Footing displacements Embankment pressures
Chadd Creek 114-in. SPP, 89-ft fill	140	Shaped	Method B		Peripheral pressures Wall strains Embankment pressures Embankment settlements
Apple Canyon 108-in. twin SPP's, 167-ft fill	137	Shaped	Method A		Peripheral pressures Wall strains Embankment pressures Embankment settlements
Mountainhouse Creek 84-in. RCP's, 140-ft fill	194	Shaped flat (sand & embankment); styrofoam concrete cradle	Method A Method B, pea gravel graded aggregate embankment material	4000D & 1000D	Peripheral pressures Internal strains Displacements Embankment pressures Embankment settlements
Cedar Creek 22-ft RC arch, 205-ft fill	160		Method A Method B	Standard & special	Peripheral pressures Internal strains Displacements Embankment pressures Embankment settlements
Soil pressures on buried conduits	16	Theoretical analysis & model studies			Displacements
Proposed Project:					
Culverts under very high fills (200 to 400 ft)	100		Undetermined		
Total	935				

A byproduct of this phase has been another computerized analysis which predicts the pressures surrounding the arch. This program was written by Colin Brown of the University of California, Berkeley, and employs a finite element analysis to determine the effects of boundary conditions, sequence of construction operations, and the influence of the layer of compressible material surmounting the culvert (3).

Empirical results of this phase may be briefly summarized as follows:

Almost without exception, soil pressure meters which functioned properly, whether in the culvert footings or barrel, or in the embankment, and regardless of orientation with respect to the horizon, produced pressures which were linear functions of embankment depth up to the full 200-ft fill height. Pressure changes after completion of the embankment were negligible (Fig. 1).

Effective densities were computed from the pressure-height functions. For this phase of the project, where the pressure-height function was linear, the effective density was calculated as the slope of the curve and was constant for the full depth. For those phases where this function was not linear, the effective density was computed using the following equation:

$$E.D. = \frac{\Delta P}{\Delta H} \times 144 \text{ pcf}$$

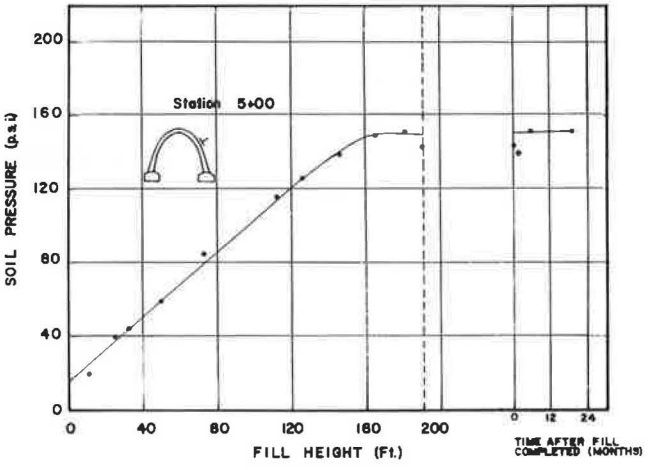

Figure 1. Typical soil pressure-embankment height function for San Luis Reservoir arch (special section, Method B, baled straw, backfill).

where ΔP is the net increase in pressure from the time the embankment is at the level of a given meter until the fill reaches a height, ΔH, above that meter. The plotted values are thus average, rather than instantaneous, effective densities.

Distributions of effective densities around the barrel periphery are shown in Figures 2 and 3.

Effective densities acting on the culvert were vastly different from those used in design. Horizontal densities were much larger; vertical densities, primarily as a result of the layer of straw, much less than had been assumed. Plots of densities acting around the barrel periphery indicated pressure maxima at the springing lines, at the crown, and halfway up the arch, with pressure minima in between.

Pressures observed on three sides of the arch at two stations indicated effective densities of 60 to 70 pcf acting horizontally, 80 to 90 pcf acting at 45 deg, and 62 to 65 pcf acting vertically. Measurements on the fourth side were 105 pcf acting horizontally and 118 pcf at 45 deg. One density near the crown temporarily fell to 42 pcf about a month after embankment completion.

California arch culvert designs have heen based on assumed vertical effective densities of 120 pcf, horizontal densities three-tenths as large or 36 pcf. Specifications permit using 70 percent of the actual weight of earth to effect an increase of allowable design dead load stresses 40 percent more than allowed for live load. The prototype was designed for 84 pcf acting vertically and 25 pcf acting horizontally.

Average overall effective densities acting downward on the culvert, computed from total downward components of pressure forces acting on the barrel and upper footing surfaces and from upward forces on the lower footing surfaces, were 76 to 95 pcf, although the most representative figures ranged from 76 to 83 pcf.

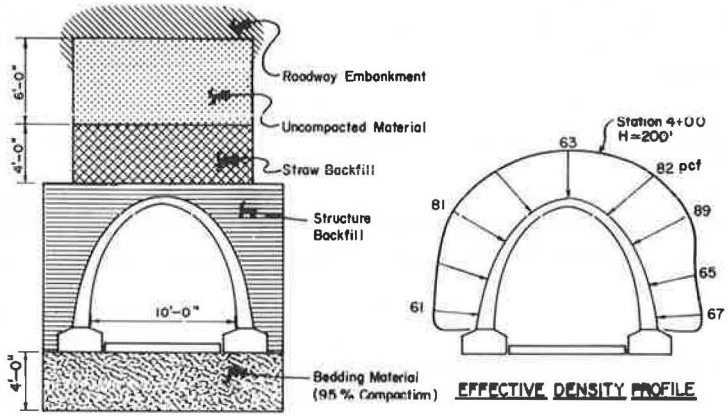

Figure 2. Effective density profile for Station 4, San Luis Reservoir arch (special section, Method B, baled straw, backfill).

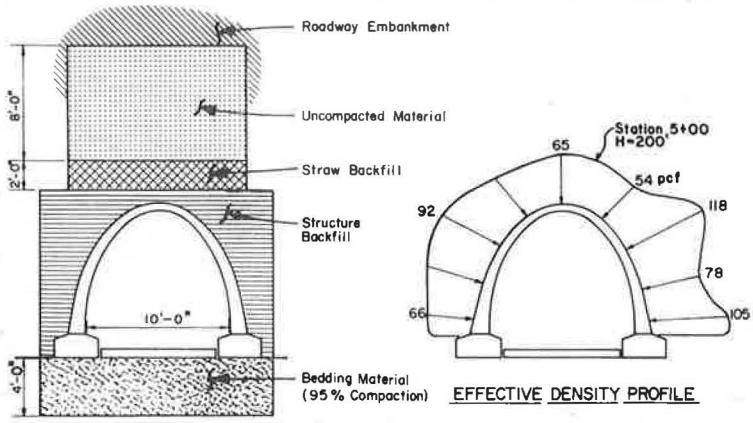

Figure 3. Effective density profile for Station 5, San Luis Reservoir arch (special section, Method B, baled straw, backfill).

Vertical effective densities in the embankment 13 ft from the centerline ranged from 84 to 266 pcf. Densities at 30 ft from the centerline, measured at two locations, were 310 and 740 pcf. The latter figure probably is erroneously high as a result of a concentrated bearing on the Terzaghi-type meter from which it was obtained. The remaining measured embankment densities, though significantly greater than the actual embankment density, are in line with observations at other locations where Method B backfill has been employed, demonstrating dramatically the increases in pressure in the "exterior prisms" as vertical shear forces transfer the load of the settling "interior prism" thereto.

Phase 3—Posey Canyon—Results observed to date at Posey Canyon in part confirmed, and in part controverted, those observed at San Luis. Functioning soil pressure meters at San Luis indicated linear relationships between pressures and embankment depths. Some meters at Posey Canyon indicated distinctly curvilinear functions while others produced linear functions with definite discontinuities.

The most pronounced curvilinear functions were observed at Station 5, where a layer of baled straw was placed around the periphery of the barrel. The increase of effective density acting on the barrel with increasing height undoubtedly results from the curvilinear stress-strain function exhibited by baled straw, which transmits greater soil pressures as it becomes increasingly compact.

A number of soil pressure meters exhibited linear pressure-depth functions up to the point where the embankment reached a height of 130 ft in early November 1966. The November readings and those taken subsequently frequently departed radically from the original linear functions. In some cases, the slope remained the same, while the pressure levels changed; in other instances, there were discontinuities both in slopes and pressure levels. These discontinuities are thought to have resulted from changes in the soil shear strength as the embankment became saturated with heavy rains which began in November.

Figure 4 is the pressure-height plot for Station 7, where no special backfill treatment was employed. Comparing the various curves, it is evident that the effect of saturating the soil was to produce pronounced decreases in effective densities acting vertically and increases in those acting horizontally—effective densities acting at 45 deg at the mid-height of the culvert remained virtually unchanged.

The published curves are not to be construed as typical. At some stations, the increases in soil pressure following saturation were only temporary. At some stations there was no evidence of leveling-off of pressures when the full embankment height was attained. Space limitations preclude publishing all the pressure-height curves at the present time.

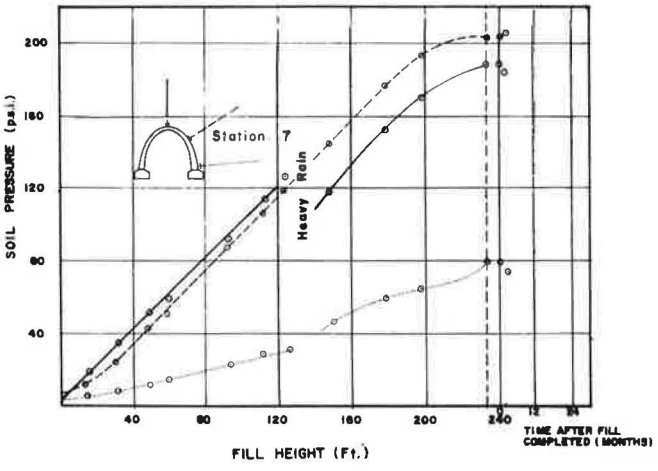

Figure 4. Soil pressure-embankment height function for soil stressmeter at crown, Station 7, Posey Canyon arch.

Calculated effective densities as they were distributed around the arch are plotted in Figures 5 through 9. Several characteristics of the curves are worth noting.

At Station 7 (Fig. 5), with no special backfill treatment, the distribution of effective densities was observed to be somewhat in line with that stipulated in the specifications (120/36), although the magnitudes of the densities were, at two stations, considerably greater.

At Station 6 (Fig. 9), where a horizontal layer of straw surmounted the arch, the computed density distribution was similar to that at San Luis, although the vertical and horizontal densities were considerably less than those observed at San Luis.

Station 5 (Fig. 8), where a bale thickness of straw was placed around the entire barrel periphery, showed the most promise, inasmuch as the lateral pressures were almost negligible and vertical densities were about half that of the embankment.

The observed pressure distribution at Stations 1 and 2 (Figs. 5 and 6), comprising standard and special structural sections, respectively, differed inappreciably from one another, except that effective densities acting on the more rigid section may have been slightly greater. The effective density distributions at these three stations, where no special backfill treatment was employed, are somewhat comparable to the 120:36 pcf ratio which has been used in design, except that observed vertical densities are greater than the design figures.

At Station 4 (Fig. 7), where a layer of uncompacted soil surmounted the arch, the vertical densities acting at the crown were little less than under Method A conditions; however, comparisons with Stations 1, 2, and 3 indicate greatly decreased densities 2 or 3 ft from the crown on either side. Horizontal densities differed little among the four stations.

In general, the effective densities acting on the right side of the arch exceeded those on the left. This phenomenon probably was influenced by boundary conditions since the right slope of the canyon, over much of the culvert's length, was nearly unbroken, whereas the left slope was characterized by a natural bench 30 to 50 ft above the stream level, which was converted into a haul road during construction. It is not unlikely that such discontinuities provide some support for the embankment, inhibiting its full settlement, and decreasing acting pressures below the broken slopes.

Readings for soil stressmeters placed in the embankment 6 ft above the crown and 8 to 20 ft out from the culvert centerline were also converted to effective densities. Many of these readings were erratic after the onset of heavy rains in November, so the

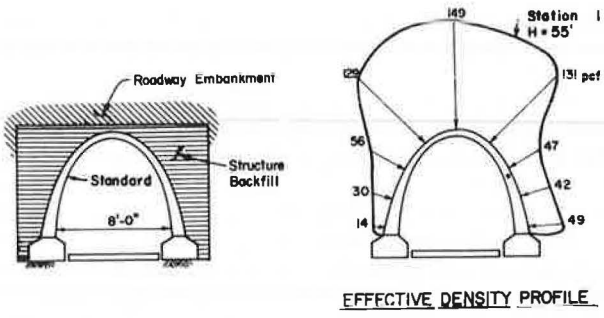

Figure 5. Effective density profile at Test Station 1, Posey Canyon arch (standard section, Method A backfill).

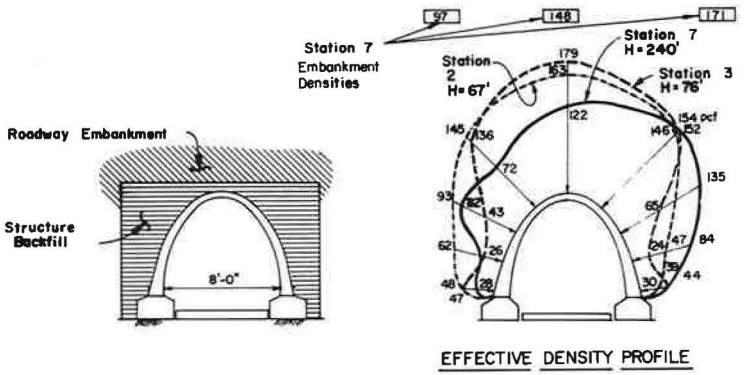

Figure 6. Effective density profiles, Stations 2, 3, and 7, Posey Canyon arch (special section, Method A backfill).

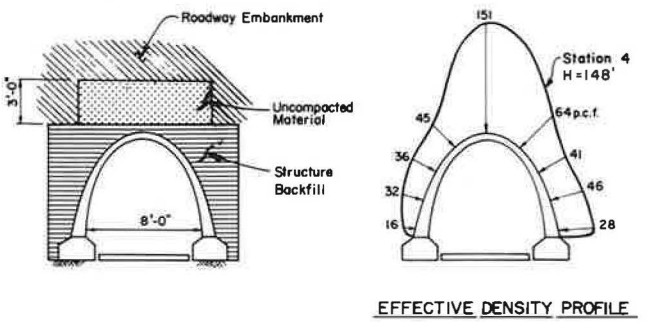

Figure 7. Effective density profile, Station 4, Posey Canyon arch (special section, Method B, uncompacted soil, surmounting culvert).

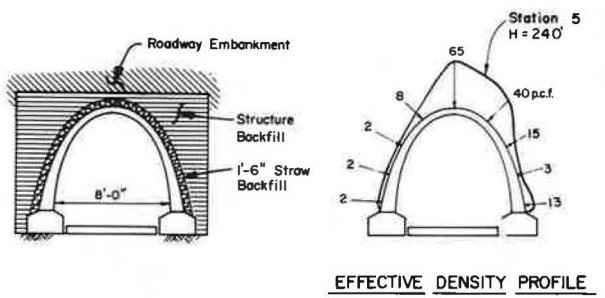

Figure 8. Effective density profile, Station 5, Posey Canyon arch (special section, Method B, baled straw surrounding culvert).

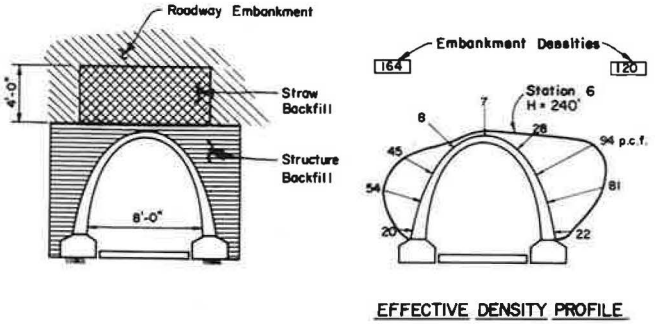

Figure 9. Effective density profile, Station 6, Posey Canyon arch (special section, Method B, baled straw, surmounting culvert).

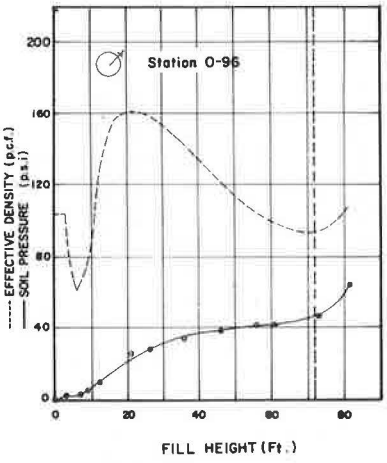

Figure 10. Soil pressure and effective density-embankment height functions at midpoint of upper quadrant; Chadd Creek steel structural plate pipe, Station 0-96 (Method B, baled straw, surmounting culvert).

pressures at the 120-ft level have been used in computing densities (Figs. 6 and 9).

Seven of the measured effective densities are appreciably higher than the embankment density, which approximated 120 to 130 pcf. Some of these excessive densities may have resulted from the longitudinal and transverse distribution of the weight of the interior prism over the straw layers to the exterior prisms. As mentioned previously, this phenomenon was observed at San Luis and Chadd Creek.

Pipe Culvert Research

Soil pressures and effective densities have been plotted as functions of embankment depths for the structural plate pipes at Chadd Creek and Apple Canyon. At the time of writing, the rigid pipe culvert study is still in its early stages.

Flexible Pipe Research (Phase 1—Chadd Creek)—Figure 10 is a plot of soil pressure and effective density as functions of embankment depth for the upper octant point on one side of the pipe. Marked similarities of configuration between symmetrically oriented meters on the left and right sides were observed. Similar configurations occurred for other locations; however, amplitudes of variation differed greatly among various octant points.

The effective density plots clearly demonstrate that, in the case of a flexible pipe using Method B backfill, design criteria may vary greatly with ultimate embankment depth, and more critical conditions may occur at lower depths.

A certain similarity of configuration of the effective density-height relationships for all orientations was evident, with distinct density maxima occurring with 20 to 30 ft over the meters, and minima with 70 to 90 ft over the meters.

Densities acting on the crown, under the straw, and at the ends of the horizontal diameter were sub-hydrostatic and remained less than 60 pcf. Super-hydrostatic densities as great as 160 pcf were observed at the upper quadrant points; those observed at the invert were well over twice the embankment density. The aforementioned densities were maximum values observed at the 20 to 30-ft levels. All observed densities except that at the invert were sub-hydrostatic for the maximum fill height.

Effective density profiles are plotted for the three stations in Figure 11, which shows large pressure bulbs at the invert and midpoints of the upper quadrants, with distinct minima at or just below the ends of the horizontal diameter and under the straw. With increasing depths, maximum densities decrease, and minima increase, so that some tendency toward a more uniform distribution is indicated.

Flexible Pipe Research (Phase 2—Apple Canyon)—Figure 12 depicts a typical soil pressure-embankment depth and effective density function for the crown of one of the 108-in. twin culverts at Apple Canyon. Of particular significance is the increase in observed pressure after fill completion on the periphery of this steel structural plate pipe. The effective density increased from 120 to 160 pcf in the period of a year after the fill was placed. This phenomenom was observed at other points about the periphery with overall increases ranging from 30 to 60 percent.

Figure 13 shows the effective density profile for Station 7+25 at the maximum fill height of 60 ft, and at Station 10+00 for the 160-ft fill height. It is evident that the structural behavior of the Apple Canyon pipe with Method A backfill differs radically from that of the Chadd Creek pipe where the baled straw was used. The Apple Canyon pressure-height curves are essentially linear, with some decreases in effective densities beginning at the 100-ft level. A slight upward curvature of some curves was evident for low depths of cover. The radical changes in effective density which accompanied

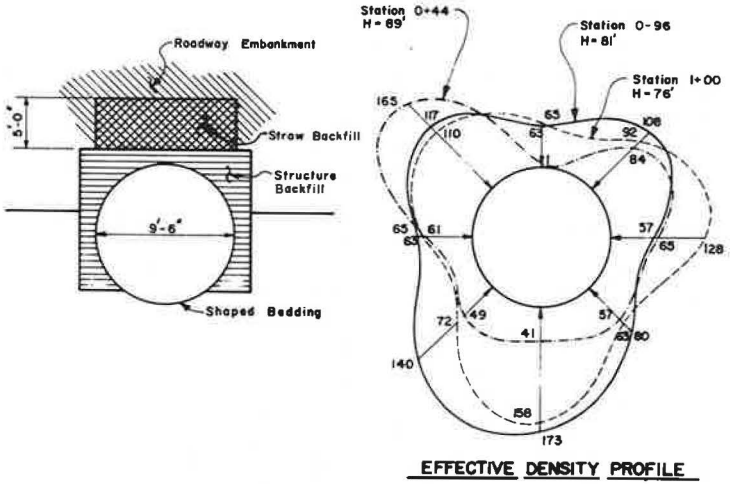

Figure 11. Effective density profiles, Stations 0+44, 0-96, 1+00, Chadd Creek steel structural plate pipe (Method B, baled straw, surmounting culvert).

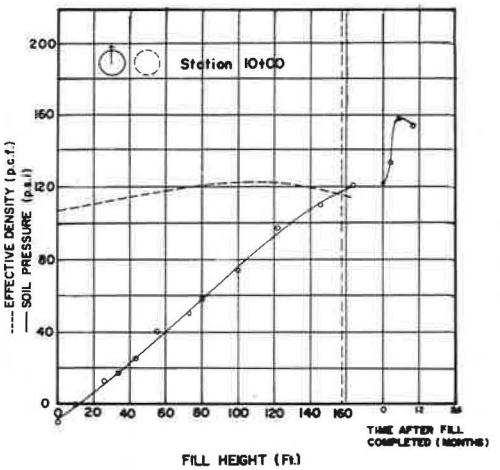

Figure 12. Soil pressure and effective density-embankment height functions at crown; Apple Canyon, 108-in. steel structural plate pipe, Station 10+00 (Method A backfill).

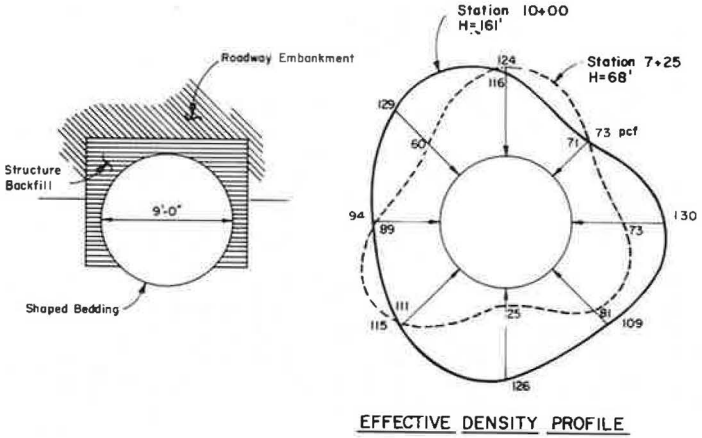

Figure 13. Effective density profiles for the Apple Canyon, 108-in. structural plate pipe (Method A backfill).

the use of Method B backfill at Chadd Creek were absent at Apple Canyon, and the Apple Canyon curves were very similar to those for Station 7 at Posey Canyon, where Method A backfill was employed. Thus, the shape of the pressure-height functions for the flexible culvert without straw were comparable to those for a rigid arch; however, the distribution of effective densities was very different, approaching a more uniform configuration around the pipe periphery.

In general, the pressure-height functions for meters surrounding rigid structures level off as soon as the maximum fill height is reached. Observations to date indicate that large changes in soil pressure acting on a flexible pipe may continue after completion of the fill over the meter.

CONCLUSIONS

For the San Luis Reservoir arch, where a rigid concrete culvert was buried in a 200-ft deep rock fill in a broad canyon:

1. The pressure-height curves were linear up to the full fill height.
2. The pressure configuration was vastly different from that assumed in the initial design.
3. Changes in effective densities after embankment completion were negligible.

The Posey Canyon culvert is a rigid arch buried in a 240-ft deep, crushed shale embankment in a V-shaped canyon.

1. Soil pressure-embankment height plots were essentially linear up to the full fill depth with exceptions as follows: (a) At Station 5, where baled straw surrounded the barrel periphery, a distinct upward curvature reflected the curvilinear stress-strain function of baled straw, which transmits greater pressures to the extrados as the straw becomes increasingly compact. (b) Some decrease in effective density began to occur when the embankment depth reached 180 ft. (c) Severe discontinuities in the linear functions were evidenced when the embankment depth reached 130 ft. These discontinuities are thought to have resulted from changes in soil shear strength due to embankment saturation with the onset of heavy rains.
2. For the condition where baled straw surrounded the barrel, lateral densities were negligible, vertical densities about half that of the embankment—these latter, however, would become greater proportions of embankment density with greater depths due to the curvilinear stress-strain function of the straw.

Pressure-height functions for the case where a layer of straw surmounted the arch were of somewhat the same configuration as those for the San Luis arch; however, horizontal and vertical densities were both much less than those measured at San Luis.

Where no special treatment was given to the backfill, the effective density distribution was much like the 120 pcf/36 pcf (horizontal:vertical) distribution used in design, although the vertical densities were somewhat higher. The super-hydrostatic densities are believed to result in part from the transference of load from the interior prism surmounting the straw at an adjacent station and in part from boundary conditions in the V-shaped canyon.

3. In general, effective densities increased after fill completion where the imperfect ditch was used, but remained essentially constant for stations with Method A backfill.

For Phase 1—Chadd Creek, flexible pipe research:

1. Effective density curves for a 114-in. structural plate pipe surmounted by a layer of baled straw were distinctly nonlinear. Maximum densities occurred with 20 to 30 ft of soil over the meter, minima with 70 to 90 ft over the meter. Configurations are similar for meters on the upper half of the pipe, for side meters, and for those at midpoints of the lower quadrants.
2. The effective density profiles show super-hydrostatic pressure bulbs at the invert; maxima at midpoints of the upper quadrants with densities slightly sub-hydrostatic; effective densities at the crown, sides, and midpoints of the lower quadrants about half that of the embankment, showing that the straw is effective in reducing vertical pressures at least up to full embankment depth.

3. Behavior of pressures after embankment completion cannot be evaluated at the present time.

For Phase 2—Apple Canyon, flexible pipe research:

1. For a 108-in. structural plate pipe with Method A backfill (positive projection), pressure-height curves were very similar to those observed for the rigid arch at Posey Canyon for the station with Method A backfill. Functions were essentially linear although some decrease in effective density began to occur at a lower level than at Posey Canyon, about 100 ft. The soil-structure interaction was thus very different from that where the Method B backfill was employed.
2. The effective density profile when embankment construction was complete exhibited more uniformity than in the case of any of the other structures tested.
3. Distinct increases in the effective densities have occurred during the five months since the embankment was completed. Transducer readings will continue until two years after embankment completion.

ACKNOWLEDGMENTS

This research was financed in part with Federal-aid highway funds and was conducted in cooperation with the United States Department of Transportation, Federal Highway Administration, Bureau of Public Roads. The work was accomplished by the California Division of Highways, Bridge Department, of which J. E. McMahon is the head. Instrumentation of the field prototype was performed by the California Division of Highways, Materials and Research Department, directed by J. L. Beaton.

Acknowledgment is gratefully made to E. E. Evans and L. R. Patterson, of the Bridge Department, for assistance in programming and data reduction; to F. G. Gillenwaters, P. F. Nichols, and B. L. Fraser, who designed the various prototype culverts; and to personnel of the Materials and Research Department for their efforts in providing accurate data.

The opinions, findings, and conclusions expressed in this publication are those of the authors and not necessarily those of the Bureau of Public Roads.

REFERENCES

1. Grinter, L. E. Theory of Modern Steel Structures. Vol. 2, Chap. 8, MacMillan Co., New York, 1949.
2. Davis, R. E. Structural Behavior of a Reinforced Concrete Arch Culvert. California Division of Highways Bridge Department Research Report SSR 3-66.
3. Brown, C. B. Rigid Culverts Under High Fills—Tractions on the Barrel and in the Soil. University of California Report No. SESM 66-7.

Soil Pressure Distribution on Buried Structures

DON A. LINGER, The Eric H. Wang Civil Engineering Research Facility Operated for the U.S. Air Force by the University of New Mexico, Albuquerque, and
PEDRO FERNANDEZ, Civil Engineer, Navojoa, Sonora, Mexico

This research evaluates the important variables of the soil-structure interaction problem. This problem has been defined in terms of two types of load redistribution: the load redistribution between the structure and the soil, and the pressure redistribution across the structure. The pressure redistribution on the structure was found to vary as a function of applied surface pressure and the depth of burial, whereas the redistribution to the adjacent soil was found to be dependent upon depth of burial alone. The parameters affecting the soil-structure redistribution and the structural redistribution were correlated, and the significance of each is discussed. After the pressure redistribution mechanism was established by a seating pressure, which was dependent upon the depth of burial, the final attenuation of pressure varied with the burial depth for the structural redistribution and with the square root of the burial depth for the soil-structure redistribution.

•NOT enough is known about soil-structure interaction to predict with any degree of accuracy the ultimate load-carrying capacity of culverts, pipeline casing, and other flexible thin-wall structures. In the design of such underground structures the soil pressures are usually based on empirical relationships which are not fully understood. If the loading on the underground structure is determined from classical earth pressure theory, great variations can be expected between the actual and the theoretical loading. These variations are the result of the underground structure deflecting and causing a reduction in the pressure transmitted to the structure with a corresponding increase in the pressure transmitted to the adjacent soil. This phenomenon is known as the pressure redistribution in bimaterial systems or as the arching phenomenon in soils.

In the case of an underground structure deflecting under load, the soil at the center of the roof span of the structure displaces with respect to the soil over the supports and with respect to the adjacent soil in which it is buried. Because of this differential deflection of the various parts of the structure and the relative flexibility of the soil and the buried structure, the arching phenomenon will occur as a redistribution of pressure between various segments of the structure and also as a redistribution of load from the structure to the adjacent soil. This simplification of a very complicated problem, which involves the composite action of soil and structure, facilitates study of the pressure redistribution mechanism. The results of this study have been divided into two parts:

1. The redistribution of pressure around the structure according to the relative flexibility of the structure and the adjacent soil (a mechanism which results in a greater proportion of the load applied to the soil-structure system being carried by the stiffer of the two components).
2. The redistribution of soil pressure over the structure itself according to the relative flexibility of the structure and the deflected shape of the structural system.

Paper sponsored by Committee on Buried Structures and presented at the 47th Annual Meeting.

OBJECTIVES AND SCOPE

The purpose of this study was to determine the important parameters governing the fundamental characteristics of soil-structure interaction, and to evaluate the quantitative effects of variations in the parameters on the amount and distribution of the pressure exerted on the structure by the surrounding soil.

Results have been evaluated in such a way as to separate the two soil-structure interaction phenomena: distribution of soil pressure on the flexible roof panel, and redistribution of pressure between the structure and the adjacent soil. The effects of depth of burial, magnitude of overpressure, and flexibility of the structure on these phenomena have also been evaluated.

Two simply supported beams, designed to yield a two-dimensional condition, were placed at various depths under the soil in the pressure-loading apparatus. These beams were instrumented so that the flexural strains could be measured along their length. The distribution of moment along the axis of each beam was determined experimentally. The loading condition necessary to produce this moment was calculated; and the effects of the loading pressure, the depth of burial, and the flexibility of the structure were evaluated.

HISTORICAL REVIEW

Research Studies

Several studies have been undertaken to evaluate the distribution of soil pressure on flexible underground structures. The first analytical study was made by K. Terzaghi in 1936 (1). This study, based on assumed failure planes, showed the effect of the deformation of a buried structural element on the resulting applied soil pressure. The failure planes, along which relative movements are assumed and on which shearing forces are generated, are the imaginary vertical failure planes extending upward from the sides of the deforming structure. Terzaghi also assumed that the vertical pressure on any horizontal section through the soil was uniformly distributed. However, he pointed out the limitations of these assumptions and predicted that real failure planes might be considerably different than those on which the shearing forces were assumed to occur.

In a study by Truesdale and Vey (2), the soil mass above a buried structure was treated as a gridwork of individual square elements. The structure was selected for its flexibility so that the influence of arching would be predominant. In this approach the authors treated the soil mass as a free body subjected to specific boundary forces. They showed that for an analytical solution to be used to predict structural loading over a wide range of parameters (i.e., panel stiffness, burial depth, soil type, etc.) it is necessary to account for changes in the ratio of horizontal stresses to vertical stresses as the soil and structure interact.

In recent studies, Chelapati (3) made an analytical investigation of the amount of uniform surface pressure that transferred to the adjacent material when a rigid horizontal support buried under a finite depth of elastic homogeneous material deflects downward. He obtained solutions based on the equations of plane strain in the form of infinite series. He established limits on the deflection of the support up to the point at which all the load on the support would be transferred to the neighboring material. He computed the amount of arching and the pressure distribution on the support for the mathematical model studied.

In another study, Van Horn (4) used the theories developed by Spangler (5) (the Marston theory) for determining loads on underground conduits. Van Horn extended these theories to include the effects of a static uniform overpressure and cohesion in the soil.

Design Criteria

The design of most underground structures subjected to heavy loading is based on criteria developed by Merritt and Newmark (6). The determination of the forces acting on the structure as a result of the surface loads depends on the type of structure (flat

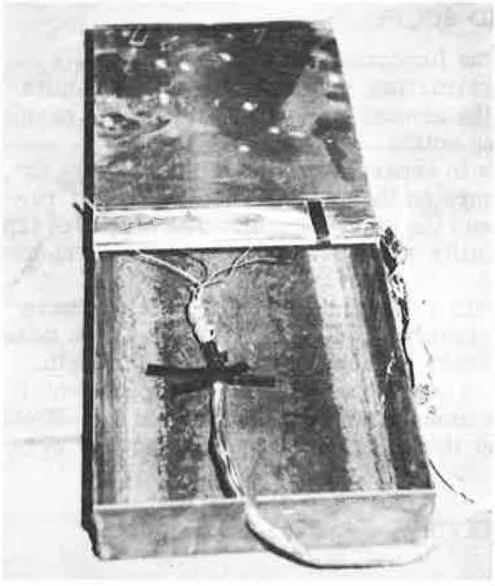

Figure 1. Model structure.

slab, arch, or dome), the shear strength of the soil, and the depth of burial. The design criteria were based on the small amount of data describing the response of underground structures and can be considered as usually conservative estimates of the actual response.

Other research conducted at the Research Institute of the Illinois Institute of Technology for the U. S. Air Force has led to the development of analytical expressions relating soil, structural, and blast-loading parameters to the failure of initially flat, buried roof and wall panels (7). This theory considers structural failure under deformations sufficiently large to mobilize the resistance of the soil. It assumes that the buried structure will tend to deform under the soil pressures, but that collapse will not occur unless the soil can move with the panel to maintain the pressures. Since soil fails in shear, to obtain large relative movements of the soil, the shearing stresses in the soil are mobilized in the formation of the pressure redistribution mechanism. The shearing resistance in the region of soil surrounding the panel is limited by the load-deformation characteristics of the structure, since shearing resistance depends, in general, on the stress level. As the panel begins to yield, the soil-shearing resistance is mobilized.

In the IITRI research, no attempt was made to evaluate pressure distribution, but assumed pressure distributions were used in an attempt to correlate the theories with experimental results. Many questions concerning theory and design were raised in the IITRI study; among the most important are the problems of the actual pressure distribution on the structures and the differences between rigid and flexible structures. In an attempt to answer these questions, the following research was undertaken.

EXPERIMENTAL CONSIDERATIONS

Test Models

In designing the model structures which were instrumented and buried in the loading apparatus, consideration was given to obtaining large deflections so as to have a pronounced arching effect in the soil. These structures were approximately 24 in. long, 10 in. wide, and 4 in. deep. A continuous aluminum plate, 24 in. long, served as the roof panel of the model structure. A beam section, 2 in. wide, was cut from the middle of the plate and instrumented to measure the moment along the beam length, which was also the width of the model structure (Fig. 1).

The flexural section or test segment of the roof panel was cut out to eliminate the three-dimensional plate effect and thus yield an idealized two-dimensional structure system.

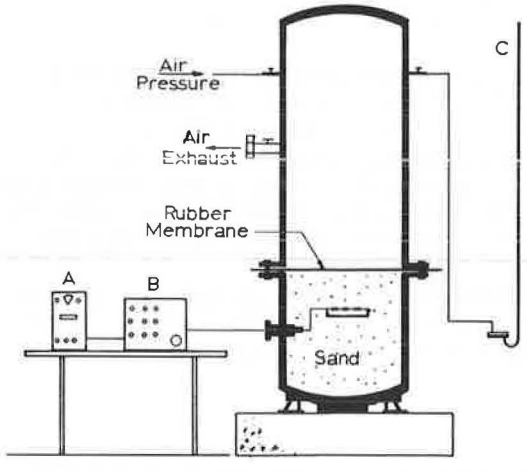

Figure 2. Experimental apparatus used to load the buried structure.

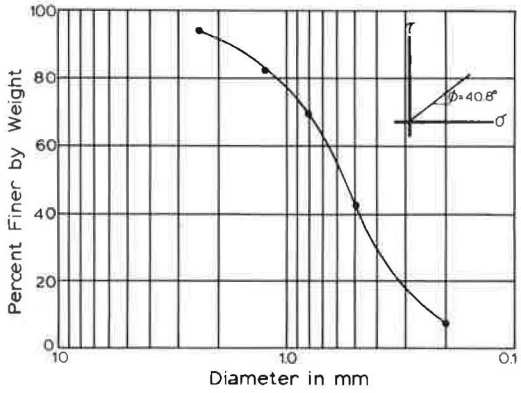

Figure 3. Properties of soil.

The test segments were 10 in. long by 2 in. wide. The flexibility of the structure was varied by using two aluminum roof panels: one was constructed of $^{3}/_{16}$-in. thick plate and the other, of $^{1}/_{4}$-in. thick plate. The instrumented test beams were at the center of the model structure roof panel. The aluminum roof panel rested on a fixed steel channel, 24 in. long, in such a manner that the channel legs supported the roof panel and test beam. The length of the structure system was believed to be large enough to ensure a two-dimensional soil deformation and a two-dimensional soil-structure interaction system insofar as the response of the instrumented test beam was concerned.

Instrumentation of Model Structure

Each beam section was instrumented with 8 strain gages, 4 on top and 4 directly opposite on the bottom along the length of the 10-in. beam. Gages were placed at the center of the beam, and at distances of approximately 2, 3, and 4 in. from the center. Because of symmetry only half of the beam length was instrumented.

Type A-7, SR-4 strain gages were used. The surface at each gage location was ground smooth with a portable grinder and cleaned with acetone before bonding the gages to the beam section of the roof panel. Duco cement was used as the bonding agent in attaching the gages to the aluminum plates. The gages were then connected to a BLH model N strain recorder through a Baldwin 20-channel switching unit (A and B in Fig. 2) to facilitate easy reading of the four strain bridges. The strain gages, located opposite each other on the top and bottom of the beam section, were placed on adjacent legs of the Wheatstone bridge so as to eliminate any axial strains present in the beam and to double the sensitivity of the flexural strains. Strains were read to the nearest 5 μ-in./in. Figure 1 shows the instrumented model structure ready to be placed in the pressure-loading apparatus.

Properties of Soil

The soil used was a dry, clean, medium sand whose grain-size distribution is shown in Figure 3. The angle of internal friction of the sand (ϕ) was found to be 40.8 deg from triaxial tests. The resulting Mohr envelope is also shown.

The Simulator

The simulator or pressure-loading apparatus is an airtight steel cylinder, 8 ft high and 30 in. in diameter. The bottom half of the simulator in which the model structure was buried is filled with the soil material and is approximately 24 in. deep. The upper half of the simulator is used to provide the air pressure for surface loading. The simulator is constructed for the application of dynamic loads with an explosive gas mixture detonated in the upper half. However, in this study only static surface pressures were used; and this type of loading was obtained by introducing static air pressure in the upper cylinder, which exerted a pressure through an airtight membrane to the soil in the lower half (Fig. 2). The applied air pressure was measured by a mercury manometer (C in Fig. 2). The model structure was placed inside the lower half of the simulator at depths varying from 0 to approximately 10 in. The soil around the structure was carefully tamped with a vibrator to eliminate any layering effect and to provide a homogeneous soil mass. A thin rubber membrane, located on the surface of the soil, separated the air pressure from the soil and assured the application of the air pressure as an intergranular pressure on the soil grains and not as a pore pressure.

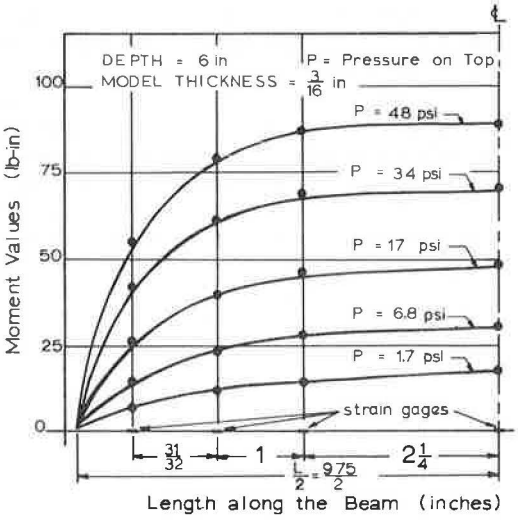

Figure 4. Experimental distribution of moment along roof panel.

ANALYTICAL CONSIDERATIONS

In Terzaghi's arching theory, a uniform displacement is assumed along the yielding horizontal strip supporting a bed of sand. Terzaghi predicted a decrease in the total load on such a horizontal strip as it displaces and that the load arches away from the center toward the supports. This redistribution is even more important in a real world structure since, when a buried structure deforms under loading, the center of the roof displaces a larger amount than the supports. The roof panel and the overlying soil then have a continuously varying displacement across the entire span rather than a uniform displacement. Therefore, the shearing planes induced in the soil by the relative deformations will extend over the length of the roof panel and will not be concentrated at one point, i.e., at the support, as assumed by Terzaghi (1) and Spangler (5). These varying displacements across the structure will result in redistribution of pressure over the structure, and it is obvious that the load arches away from the center toward the supports.

It was found in this research that the moment diagram varied with the pressure, deflection, and depth of burial. It was also found that the moment diagram flattens and approaches a trapezoidal shape or a parabolic curve of higher degree as the surface load increases and the panel deflects. An example of the change in the moment diagram is shown in Figure 4. Therefore, it was assumed in this study that the load redistribution mechanism transferring load away from the center toward the supports is the result of a nonuniformly varying load with a maximum at the supports and a minimum at the center of the span in the form of a parabolic pressure distribution.

Theoretical Loading

The parabolic pressure distribution assumed in this study is shown in Figure 5. This pressure distribution, in which the variables are the degree of the parabola (n) and the ratio of the pressure at the center to the pressure at the edge (α), yields generalized higher order moment equations as found experimentally. The general equation for the parabolic load distribution is

$$w = \frac{(-2)^n (1 - \alpha) W}{L^n} \left(x - \frac{L}{2} \right)^n + \alpha W \qquad (1)$$

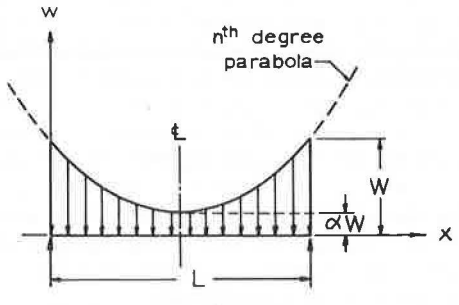

Figure 5. Assumed load distribution on structure.

where

- w = loading on the structure/unit length;
- L = length between supports = 9.75 in.;
- n = degree of parabola = 0, 1, 2, 3, 4,...;
- W = maximum load at supports/unit length;
- α = ratio of load at center to load at supports; and
- x = distance along the beam from 0 to L/2.

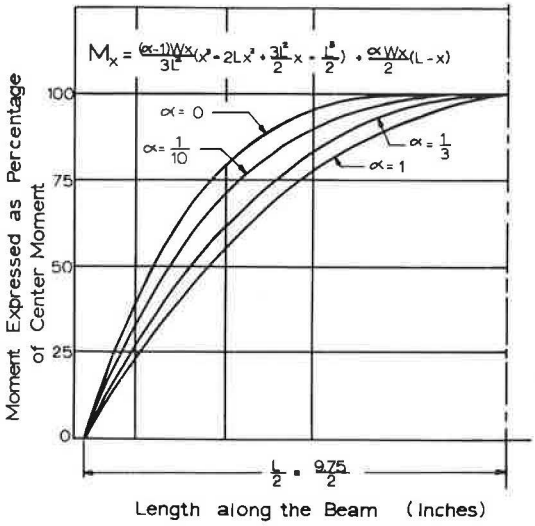

Figure 6. Family of theoretical moment curves under parabolic loading (n = 2).

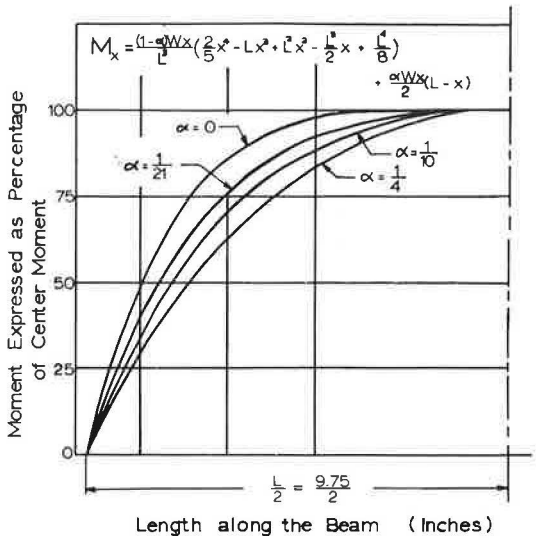

Figure 7. Family of theoretical moment curves under parabolic loading (n = 3).

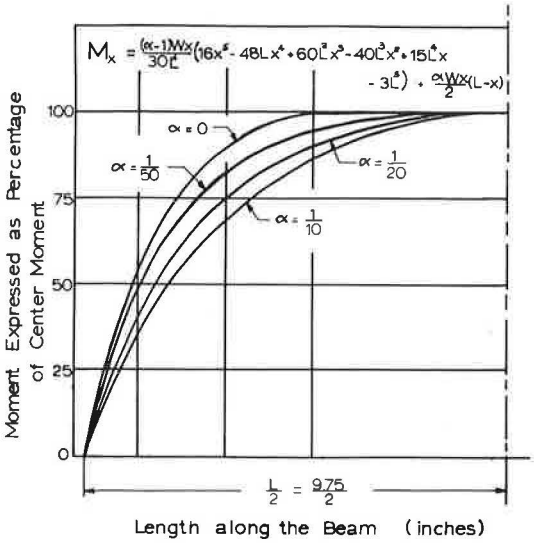

Figure 8. Family of theoretical moment curves under parabolic loading (n = 4).

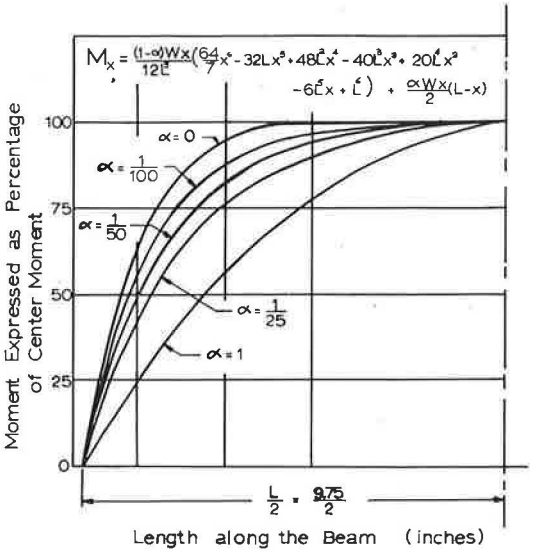

Figure 9. Family of theoretical moment curves under parabolic loading (n = 5).

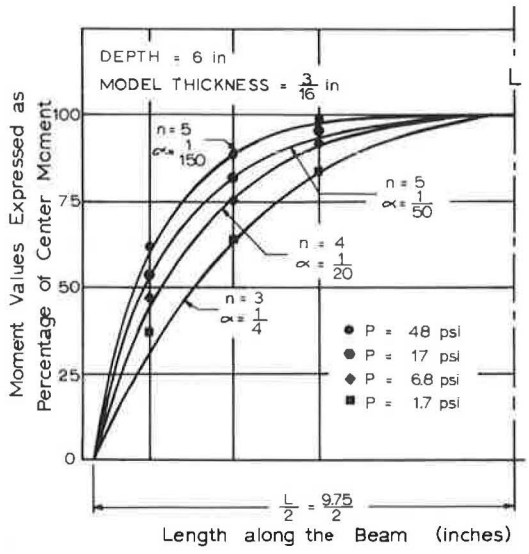

Figure 10. Fitting experimental moment values to theoretical moment curves.

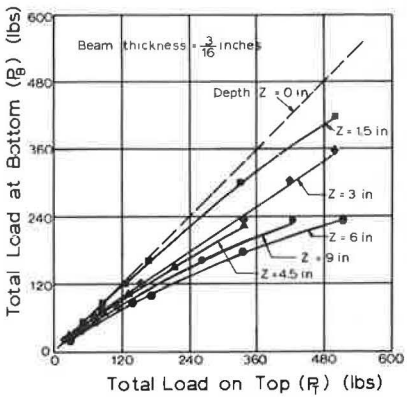

Figure 11. Soil-structure redistribution of total load with depth of burial ($t = 3/16$ in.).

Eq. 1 for the assumed loading was then integrated twice, yielding an equation for the moment in terms of the unknowns α and n. The resulting family of curves was plotted by assigning several values to α (between 0 and 1) for each value of n (from 2 to 5) and then plotting the resulting moment diagram as a percentage value of the center moment as ordinate and the length x along the beam as abscissa, as shown in Figures 6, 7, 8, and 9. The experimental moment curves were then compared with the theoretical moment curves. The best fit of the theoretical curves to the experimental data was used as the criteria for obtaining the load distribution factors α and n as shown in Figure 10.

Once a moment equation was obtained which best fit the experimental points, the corresponding load distribution diagram was assumed to depict the actual soil pressure distribution on the roof of the buried structure for the evaluation of the soil-structure and structural load redistribution mechanism formed by the deflection of the structure.

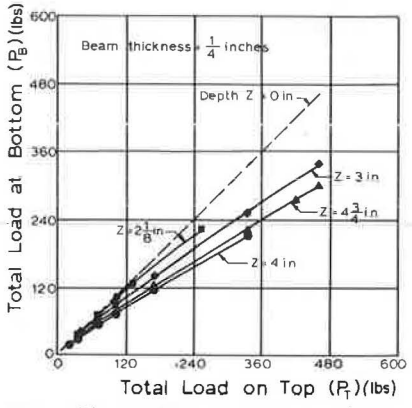

Figure 12. Soil-structure redistribution of total load with depth of burial ($t = 1/4$ in.).

Evaluation of Soil-Structure Redistribution

The first integral of the theoretical best-fit load diagram was used to determine the total load on the structure. This total load on the structure was then compared with the sum of surface pressure over the horizontal projection of the underlying structural element to determine the soil-structure redistribution.

Evaluation of Structural Redistribution

The pressure redistribution on the structure or structural redistribution is indicated by the factors α and n. The coefficient α indicates the total amount of pressure distributed away from the center of the beam. The factor n is a function of the change in the pressure diagram from the center to the edge of the the beam. The factor n is a function of the change in the pressure diagram from the center to the span and is indicative of the rate of change of the redistributed pressure. It is apparent that various combinations of α and n yield approximately similar moment diagrams, but continuity was found to occur in the values with the magnitude of n increasing

and α decreasing, as the redistribution mechanism became more effective. Moreover, a smooth transition in values of α and n should occur, but because the graphically fitted moment curves were derived from Eq. 1 using whole integers for n and $1/\alpha$, a step variation was often apparent and has been averaged out in evaluation of the results.

RESULTS AND DISCUSSION

The variation in the soil pressure on an underground structure has been separated into two basic phases: (a) the "soil-structure redistribution" which varies according to the relative flexibility of the structure and the adjacent soil, and (b) the "structural redistribution" which varies according to the degree of flexibility of various parts of the structure and the deflected shape of the structural system.

Phase I, Soil-Structure Redistribution

The experimental results are shown in terms of (P_T), the total load above the buried structure which consists of the surface overpressure plus the weight of the overlying soil, and the actual load exerted on the buried structure (P_B) as determined from summating the load distribution diagram.

Figure 11 illustrates the attenuation of the applied surface pressure (P_T) versus pressure at bottom (P_B) for different burial depths of the $^3/_{16}$-in. thick structure. The rate of the attenuation or reduction in pressure increases with an increase in the surface overpressure and with an increase in the burial depth. This is indicated by the decrease in the slope of the P_B versus P_T curve as the pressure and depth increase. If the pressure redistribution is defined as the reduction of load acting on the roof panel of the buried structure with respect to the applied surface overpressure, then at small pressures the redistribution varies from 5 to 45 percent while at higher pressures the redistribution varies from 17 to 55 percent.

For the $^1/_4$-in. thick panel (Fig. 12), the pressure redistribution for the more rigid structure is less than that for the more flexible. However, the same characteristics are noted for the effect of pressure and depth of burial for both types of structures. At small pressures from 1 to 10 psi, the redistribution in the stiffer structure varies from 5 to 30 percent. At pressures around 25-psi overpressure, the redistribution varies from 15 to 35 percent. At a depth greater than 4 in. or approximately 40 percent of the span length, there is little if any change in the attenuation of P_B with increase in depth of burial.

Both structures exhibit a maximum depth beyond which the total pressure on the structure did not continue to decrease but remained approximately constant. These larger depths of burial were not investigated because of the possibility of interaction of the soil with the restricting walls of the simulator.

Phase II, Structural Redistribution

The second basic study consists of an evaluation of the soil pressure redistribution over the structure itself, according to its degree of flexibility. The pressure redistribution of the structure was determined by the ratio of the pressure at the center of the span to the pressure at the support (α) and the rate of change of the centroid of the pressure diagram from the center to the edge of the span (n).

Pressure Redistribution (α)—Since α is indicative of magnitude of redistribution, and the formation of the redistribution mechanism depends on the soil deformation, it follows that redistribution results from the deflection of the structure. Moreover, the factor α should vary as the applied pressure varies since it is the applied pressure which causes the structure to deflect. This was evaluated by determining the relationship between the values of α for each pressure increment at each depth and at the applied surface pressure. The results are shown in Figures 13 and 14 for the $^3/_{16}$- and $^1/_4$-in. plates, respectively. It is evident that the depth of burial affects the amount of pressure necessary to form the redistribution mechanism, but once the mechanism is formed, the slope of the lines in Figures 13 and 14 yields the following relationship:

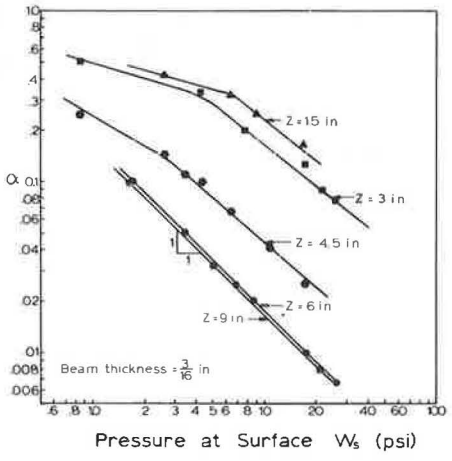

Figure 13. Variation of pressure redistribution factor (α) with surface pressure (W_S).

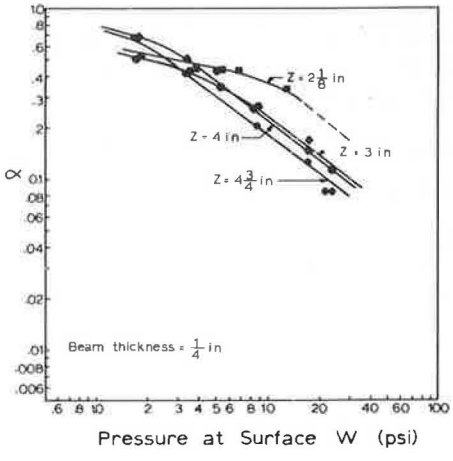

Figure 14. Variation of pressure redistribution factor (α) with surface pressure (W_S).

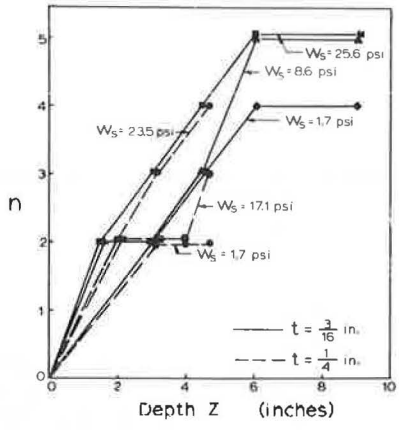

Figure 15. Variation in rate of pressure redistribution (n) with depth of burial (Z).

$$\alpha = C_0 (W_S^{-1})$$

where the constant C_0 depends on the depth of burial, and W_S is the applied surface pressure.

It is apparent from a comparison of these figures that the constant C_0 is considerably affected by the stiffness of the structure as well as the depth of burial. The redistribution mechanism can, therefore, be formed for a flexible structure at only a fraction of the burial depth necessary for a more rigid structure.

Rate of Redistribution (n)—Since n indicates the rate of redistribution, its value should depend on the degree of formation of the redistribution mechanism and the depth of burial which will determine the potential capacity of such a mechanism. For the assumptions made concerning the type of load after redistribution, the factor n determines the rate at which pressure is distributed to adjacent beam segments. This effect is shown in Figure 15, which indicates the increase in the rate of pressure redistribution which occurs as the depth of burial increases. The lower values of n for the lower pressures show the smaller rate of redistribution which occurs in the early formation of the redistribution mechanism. As the pressure and, hence, deflection increase, the rate of redistribution increases to a maximum value which depends on the potential capacity of the redistribution mechanism or on the depth of burial. The values should form a smooth curve, but the method of fitting the moment diagrams yielded abrupt changes in the values of n because of the whole numbers used for the parabolic degrees. It is also evident that both the stiffer and more flexible structures exhibited similar rates of pressure redistribution (n values) at each depth, although the stiffer structure required more surface pressure to form the pressure redistribution mechanism. In general an average value of n can be taken as

$$n = \tfrac{3}{4} Z$$

with a maximum value of n = 5.

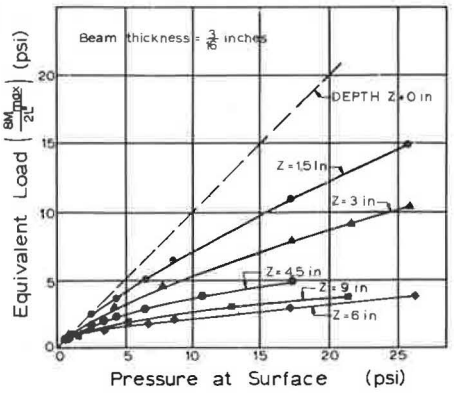

Figure 16. Variation of structural redistribution of pressure with depth of burial ($t = 3/16$ in.).

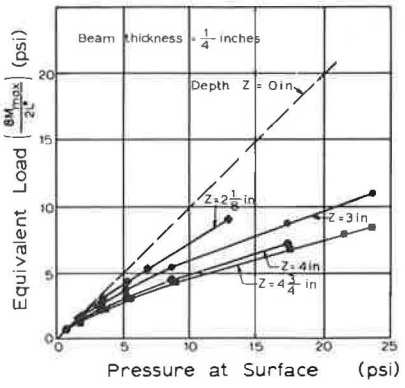

Figure 17. Variation of structural redistribution of pressure with depth of burial ($t = 1/4$ in.).

Overall Structural Redistribution for Design Purposes

The corresponding reduction in pressure at the center of the span, because of the redistribution to the edge and the rate of redistribution, results in a reduced value of design pressure for a buried structure. The overall effect of the redistribution of pressure can be evaluated by determining the equivalent uniform load necessary to obtain the same maximum moment measured experimentally at the center of the span. This method of analysis assumes that the load yields a second-degree moment diagram, but inasmuch as only the maximum value is used in design, little is lost by this assumption. The equivalent uniform load was obtained by

$$W_{eq} = \frac{8M_{max}}{L^2}$$

where M_{max} is the maximum moment at the center of the span (L).

The variation in the equivalent uniform load at various depths of burial for increasing surface pressure is shown in Figures 16 and 17. The results indicate an equivalent value of uniformly distributed load which can be used in design to yield the same moment at the center as the actual nonuniformly varying parabolic pressure distribution. The slope of the curves has the same significance as discussed previously for Figures 11 and 12. The same increase in attenuation is indicated for increasing surface pressure and depth of burial. At surface pressures in excess of 5 to 10 psi, the redistribution mechanism is completely formed and the rate of redistribution in this steady-state condition is dependent on the depth of burial.

To show the rate of formation of the redistribution mechanism, the ratio W_{eq}/W_s was determined at various levels for each depth of burial. The results are shown in Figure 18, in which the resulting straight-line variation in attenuation (using log-log coordinates) yields the following relationship:

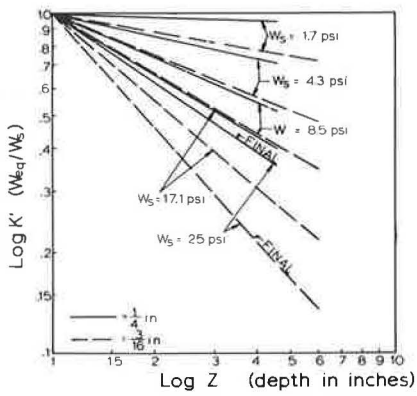

Figure 18. Attenuation of equivalent uniform pressure with depth and surface pressure.

$$W_{eq} = \frac{W_s}{Z^r}$$

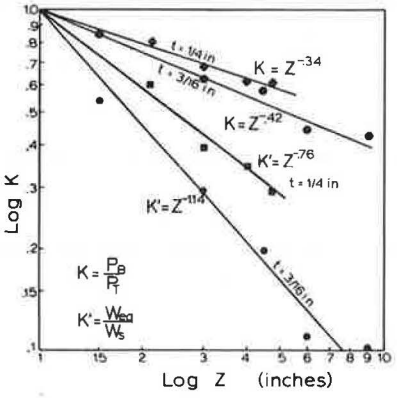

Figure 19. Attenuation of P_B and W_{eq} loads after formation of pressure redistribution mechanism.

where r is a constant which depends on the surface pressure and has values between 0 and 1. Very small surface pressures will result in values of r greater than zero; however, the pressure necessary for large values for r ($r \geq 1$) probably depends on the flexibility of the structure and may not be attainable for relatively stiff structures.

Comparison of Structural and Soil-Structure Redistribution

As evidenced by the variation in total pressure as well as the pressure distribution on a buried structure with the depth of burial, surface pressure, and flexibility, the soil-structure interaction problem is very complex. It has been shown that the formation of the pressure redistribution mechanism depends on the relative flexibility of the structure. It has also been hypothesized that both the total pressure received by the structure and the amount of pressure equivalent to a uniform load in producing moment reach a steady-state condition of attenuation once the redistribution mechanism is completely formed. However, the amount of attenuation attributable to each type of redistribution is different. The final rate of redistribution for each phase of the soil-structure interaction problem is shown in Figure 19. The upper curves indicate the attenuation factor (K) for total load (P_B/P_T), and the lower curves indicate the attenuation factor (K') for the equivalent uniform load W_{eq}/W_S for various depths of burial. The attenuation factor (K) for the total load was obtained as the final slope of the curves in Figures 11 and 12, and the attenuation factor (K') for the equivalent uniform load was obtained as the final slopes of the curves in Figures 16 and 17.

The curves in Figure 19 indicate the significantly larger attenuation resulting from the nonuniform pressure redistribution on the structure as compared to the attenuation of the total load received by the structure. Moreover, the effect of the structural flexibility is more apparent for the equivalent uniform load attenuation. In general the final loads used in the design of an underground structure can be written in the form

$$P_B = \frac{P_T}{Z^s}$$

or

$$W_{eq} = \frac{W_S}{Z^u}$$

where s and u depend on the degree of formation of the pressure redistribution mechanism which, in turn, is a function of the relative flexibility of the structure and the adjacent soil. For the structures tested and the soil used, the maximum values of s and u for the more flexible ($^3/_{16}$ in. thick) structure were found to be approximately $^1/_2$ and 1, respectively. These values yield a maximum attenuation condition of

$$P_B = \frac{P_T}{\sqrt{Z}}$$

and

$$W_{eq} = \frac{W_S}{Z}$$

for the structures, depths of burial, and soil used. Similar approximate design criteria for the more rigid (¼ in. thick) structure are

$$P_B = \frac{P_T}{\sqrt[3]{Z}}$$

and

$$W_{eq} = \frac{W_S}{\sqrt[4]{Z^3}}$$

CONCLUSIONS AND RECOMMENDATIONS

Conclusions

The following conclusions may be established from the results of the structures, soils, and depths of burial tested:

1. The loading on an underground structure subjected to the surface pressure can be assumed to vary as the structure deflects and the overlying soil is deformed.
2. The deformation of the soil results in a redistribution of pressure away from the flexible areas to the more rigid regions of the structure and/or adjacent soils.
3. The rate at which the redistribution of pressure (n) occurs depends on the depth of burial once the pressure redistribution mechanism forms.
4. The magnitude of redistributed pressure (α) depends on the relative deflection between the stiffer and more flexible regions and can be related to the applied pressure.
5. Once the redistribution mechanism is formed, the redistribution of pressure occurs at a constant rate and the amount of pressure redistribution is proportional to the applied surface pressure.
6. An equivalent uniform load, which can be used in design, incorporates both the rate and magnitude of redistribution and indicates that the structural redistribution is more effective in attenuating surface pressures than the soil-structure redistribution.

Recommendations

An attempt has been made to advance the basic knowledge of the response of underground structures to surface loading. Using the conclusions of this study and others, the following recommendations are made:

1. That various materials be used as fill (back-packing) around the structure to further evaluate the type of redistribution mechanism formed during the soil-structure interaction phenomena.
2. That this study be expanded to include large-scale structures for an evaluation of the scale factors and verification of design criteria.
3. That a study be undertaken to evaluate the amount of pressure necessary to form the redistribution mechanism.
4. That the effect of soil type on the soil-structure interaction problem be evaluated.
5. That the effect of time rate of loading be studied.

ACKNOWLEDGMENTS

The authors wish to express their appreciation to Emmet Laursen, Professor and Head of the Department of Civil Engineering of the University of Arizona where this study was carried out.

REFERENCES

1. Terzaghi, Karl. Theoretical Soil Mechanics. John Wiley & Sons, Inc., New York, 1943.

2. Truesdale, W. B., and Vey, E. An Investigation of Panel-Arching Effects in Noncohesive Soil. Proceedings of the Symposium on Soil-Structure Interaction, University of Arizona, Tucson, June 1964.
3. Chelapati, C. V. Arching in Soil Due to the Deflection of a Rigid Horizontal Strip. Proceedings of the Symposium on Soil Structure Interaction, University of Arizona, Tucson, June 1964.
4. Van Horn, D. A. A Study of Loads on Underground Structures. Proceedings of the Symposium on Soil-Structure Interaction, University of Arizona, Tucson, June 1964.
5. Spangler, M. G. Soil Engineering. International Textbook Co., Scranton, Pa., 1951.
6. Merritt, J. L., and Newmark, N. M. Design of Underground Structures To Resist Nuclear Blast, Vol. II, Final Report. Civil Engineering Studies, Structural Research Series No. 149, Contract No. DA 49-129-eng-312, Office of the Chief of Engineers, U. S. Army, University of Illinois, Urbana, April 1958.
7. Selig, E. T., McKee, K. E., and Vey, E. Underground Structures Subject to Air Overpressure. J. Eng. Mech. ASCE 86, No. EM4, p. 87-103, Aug. 1960.

The Modification of the Pressures on Rigid Culverts With Fill Procedures

S. PAWSEY, University of California, Berkeley, and
C. B. BROWN, Columbia University

A finite-element method of analysis for problems of plane elasticity is employed in the consideration of the pressures on a rigid culvert in which varying fill procedures are used. Five cases are dealt with and the practical effects of these procedures are discussed.

•THE forces acting on the barrel of a rigid culvert due to the dead load of a high fill have been shown to be sensitive to the construction procedures, especially the presence of inclusions of organic material (1). This feature was included in an approximate analytical method which predicted the total force on the culvert (2). Subsequently the use of the finite-element method for obtaining approximate solutions to plane problems of linear elasticity in which the presence of the hay inclusion was accounted for in the construction fill sequence allowed the pressure distribution on the culvert to be described (3, 4). This essentially incremental technique was described theoretically for problems in point-symmetry (5) and infinite-sided embankment (6), and applied to arbitrary geometry by a computer method (7). Fortunately, the methods were checked for an actual construction where the culvert was instrumented to determine empirically the surface pressures (3, 4). It was found that the analytical techniques gave an excellent picture of the pressure distribution on the rigid culvert. With this in mind a rigid culvert at Posey Canyon, Calif., was analyzed at five cross sections in which the fill height, the presence and arrangement of different materials and the degree of fill compaction were varied. By this means some understanding of the effects of these various construction devices can be obtained. Confidence in the solutions rests on the previously stated agreement between analytical and experimental results.

In this note, the fill procedures and resulting culvert forces are described and the practical implications of the analysis discussed. No effort is made to provide the analytical treament which is adequately described elsewhere (3, 4). A description of the instrumentation and the measurements to date at Posey Canyon are provided by Davis and Bacher (8).

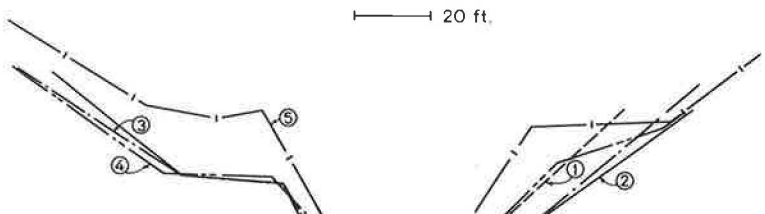

Figure 1. Earth geometry.

Paper sponsored by Committee on Culverts and Culvert Pipe and Presented at the 47th Annual Meeting.

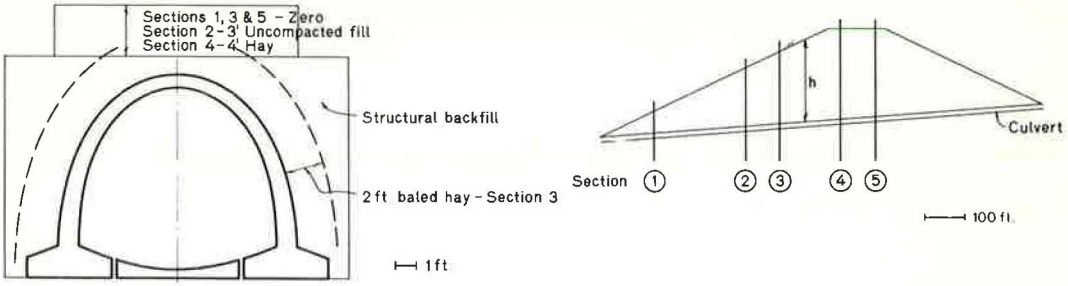

Figure 2. Culvert and fill geometry.

CULVERT AND FILL ARRANGEMENTS

The ground geometry is shown in Figure 1. The culvert was 8 ft high. Figure 2, together with Table 1, indicates the fill and culvert arrangements. Section 4 was constructed by placing the baled straw and filling around it. In the analysis the nodes at the interface between the fill and the culvert were considered to be free to move tangentially along the culvert.

The various material properties assigned to the fill materials were

$$E_{fill} = 9 \times 10^5 \text{ psf}$$
$$E_{uncompacted\ fill} = 4.5 \times 10^5 \text{ psf}$$
$$E_{hay} = 3 \times 10^4 \text{ psf}$$
$$\nu_{fill} = \nu_{hay} = 0.4$$
$$\rho_{fill} = \rho_{hay} = 120 \text{ pcf}$$

The existing ground surface and the culvert were designated as rigid.

RESULTS

Figure 3 gives a plot of the final normal pressure on the culvert at the five sections, this plot is normalized by dividing by the product of the fill density (ρ) and the fill height (h) in Figure 4.

Figures 5, 6 and 7 indicate the variation in the normal pressure on the culvert with fill height at three locations on the barrel.

TABLE 1

Section	Fill Height Above Crown, 2 (ft)	Special Procedures
1	60	None
2	152	Uncompacted material—3 ft thick (Fig. 2)
3	188	Baled straw—2 ft thick around arch (Fig. 2)
4	233	Baled straw—4 ft thick (Fig. 2)
5	228	None

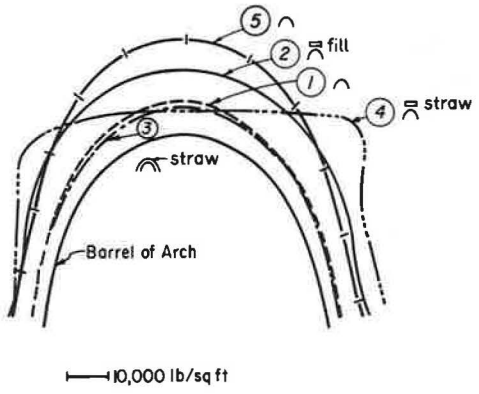

Figure 3. Normal pressure distribution.

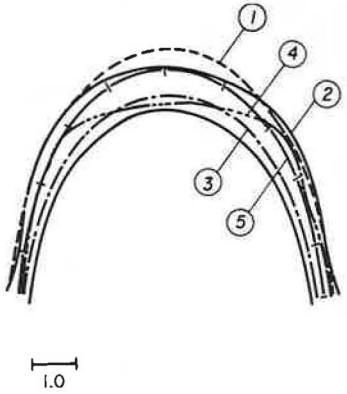

Figure 4. Normalized pressure distribution.

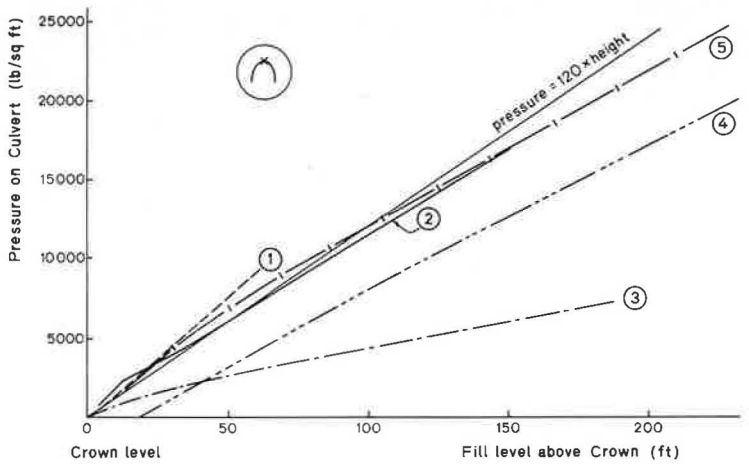

Figure 5. Variation of pressure with fill height—crown.

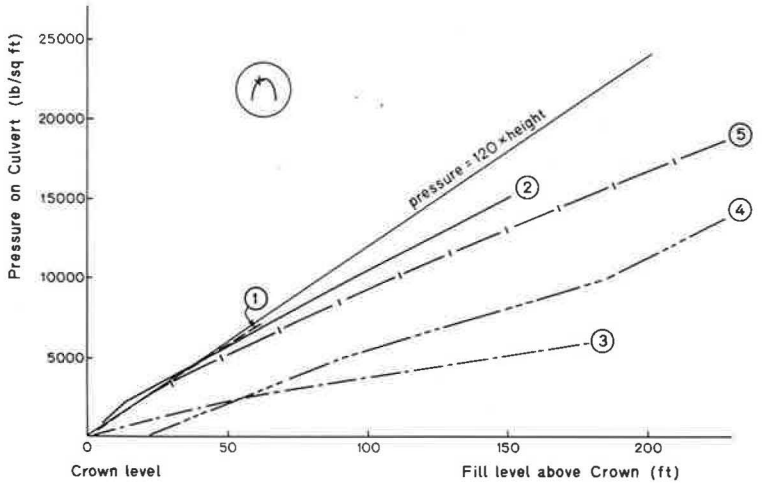

Figure 6. Variation of pressure with fill height—shoulder.

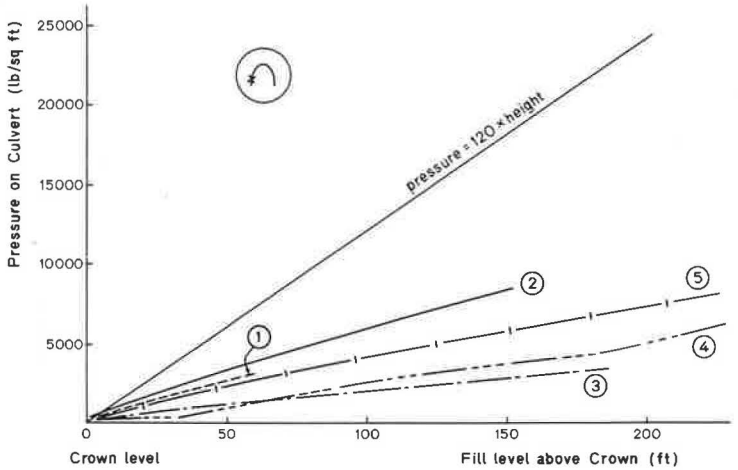

Figure 7. Variation of pressure with fill height—wall.

DISCUSSION

The reasons for modifying the fill procedures are to reduce the magnitude of the pressures on the culvert and to cause the pressure distribution to induce a more acceptable structural action on the culvert. Generally, it is most satisfactory to maintain the structural action of the culvert as an arch. This means that bending and shears due to changes of bending moment with position do not exist. Such a pressure state will depend upon the culvert geometry (i. e., for a circular cross-section the pressure should be uniform), and the alteration of the fill procedures by changing the type and arrangement of inclusions can be helpful in attaining the proper structural action as well as reducing the magnitude of the forces acting on the culvert. However, a word of warning is proper. As illustrated in references (3, 4), when an inclusion of organic material is used it is possible to modify the surface pressures on the culvert in a satisfactory manner; but, because of the change in the composition of these organic inclusions with time the pressures will continually change so that when full decomposition has occurred a most unsatisfactory pressure distribution may exist. For inclusions of hay, as in section 4, the pressure at the crown tends to fall to zero over a period of years whereas the pressures at the location of Figure 6 and further away from the crown remain unchanged. This arrangement produces bending and shear which may result in the complete change in structural action from that intended.

The fill procedures indicated in Figure 2 and Table 1 produce different pressure magnitudes and distributions on the culvert. In every case where different procedures from those of the homogeneous fill are used the ratio of the moduli of the materials of the fill is critical (3, 4). However, the establishment of the modulus of elasticity for hay and uncompacted fill has always been troublesome. The figures used here are the means of those obtained in an extensive test program by the California Division of Highways. It is believed that they insure that the analysis is relevant.

The distribution of the fill pressures are clear from Figures 3 and 4. The presence of the weaker material over the crown (sections 2 and 4) reduces the crown pressures. The straw around the barrel (section 3) provides the same distribution as the homogeneous fill (sections 1 and 5) but with markedly reduced pressure magnitudes. The manner of the variation of the pressure with fill height may be examined in Figures 5, 6 and 7. A comparison of the normal stresses over the crown in sections 1, 2 and 4 shows a progressive reduction as the modulus of the section of fill over the culvert is reduced from that of homogeneous fill (section 1) by the use of a block of uncompacted fill (section 2) or of straw (section 4). It appears that the quantity, position and assumed properties of the straw induces very severe pressure gradients on the culvert in section 4.

The two cases of homogeneous fill provide slightly different plots (sections 1 and 5). This may be attributed to the geometry of the original surface (Fig. 1) where the culvert at section 5 lies in a deep trench compared to 1.

The low pressures on the barrel in section 3 do not affect the internal soil stresses in the fill outside the straw. These stresses are much the same as in the homogeneous case (5), but much more severe stress gradients occur. Thus a likelihood of local fill failure has to be considered.

CONCLUSION

The result for the five sections considered indicated the manner in which various fill procedures will alter the pressures on a rigid culvert. This type of experience may allow a specification of fill procedure such that a desired pressure distribution is attained. The analytical technique previously developed (3, 4) can be applied to the practical situations and an estimate of the barrel pressure conditions obtained. It is necessary to be cautious about accepting such pressure figures because of their sensitivity to inclusion modulus value, earth motion and the three-dimensional aspects of the problem. However, these figures will be of guiding value in the design situation.

ACKNOWLEDGMENTS

This work was supported by the Division of Highways, State of California in conjunction with the Bureau of Public Roads. The opinions, findings and conclusions in this work are those of the authors and not necessarily those of the Bureau of Public Roads.

REFERENCES

1. Marston, A. Report to Joint Concrete Culvert Pipe Committee. Nov. 1921.
2. Spangler, M. G. A Theory of Loads on Negative Projecting Conduits, HRB Proc., Vol. 30, 1950.
3. Brown, C. B. Forces on Rigid Culverts Under High Fills. Jour. Structural Division, Proc. A. S. C. E., Oct. 1967.
4. Brown, C. B. Rigid Culverts Under High Fills, Tractions on the Barrel and in the Soil. Report No. SE SM 66-2, Structures and Materials Research, Department of Civil Engineering, University of California, Berkeley, 1966.
5. Brown, C. B., and Goodman, L. E. Gravitational Stresses in Accreted Bodies. Proc. Royal Society, London, A, Vol. 276, p. 571, 1963.
6. Goodman, L. E., and Brown, C. B. Dead Load Stresses and the Instability of Slopes. Jour. Soil Mech. and Fdns. Div., Proc. A. S. C. E., Vol. 89, No. SM3, p. 103, 1963.
7. Brown, C. B., and King, I. P. Automatic Embankment Analysis: Equilibrium and Instability Conditions. Geotechnique, Vol. 16, No. 3, p. 209, 1966.
8. Davis, R. E., and Bacher, A. E. California's Culvert Research Program—Description, Current Status, and Observed Peripheral Pressures. Highway Research Record 249, p. 14-23, 1968.

Discussion

M. G. SPANGLER, Research Professor, Iowa State University—The King James translation of the ninth verse, first chapter, of the Book of Ecclesiastes reads: "The thing that has been, it is that which shall be, and that which is done is that which shall be done: and there is no new thing under the sun." In the modern vernacular we often hear it said "there is nothing new under the sun." These were the first thoughts which came to the writer upon reading this paper, which is extremely interesting and valuable when viewed from the background of the extensive research in the field of loads on buried conduits which has been conducted over the years at Iowa State University.

In 1919 the late Anson Marston, Dean of the College of Engineering and Director of the Engineering Research Institute, conducted a load-measuring experiment on a 40-in. diameter buried conduit under 20-ft of fill. He found, to his dismay, that the actual load on the conduit was nearly double—92 percent greater than the weight of the prism of soil lying directly above the conduit. In an attempt to minimize this high load situation, he developed the Imperfect Ditch method of fill construction, which is a procedure exactly the same as that described by the authors at Section 2 of their arch culvert. An experiment conducted during the next year according to this procedure, resulted in measured loads on the conduit which were reduced by more than 40 percent compared with those measured in 1919. He reported these findings on November 28, 1921, at Chicago, Illinois, to the "Joint Concrete Culvert Pipe Committee" consisting of representatives from the: American Concrete Institute, American Association of State Highway Officials, American Railway Engineering Association, American Society for Testing and Materials, American Society of Civil Engineers, American Concrete Pipe Association, and U. S. Bureau of Public Roads.

Later he advocated increasing the compressibility of the imperfect ditch backfill by incorporating organic materials such as straw, hay, cornstalks, etc., thus anticipating the method of construction described by the authors at Section 4.

These suggestions caught on very slowly, as engineers were habitually opposed to incorporating foreign organic materials in earth fills. However, in more recent years, with heights of fill becoming ever greater as increasingly high standards for Interstate Highway construction are developed, the use of such materials has greatly increased. The writer is familiar with projects involving the use of sawdust in Texas, tree leaves and pine straw in Georgia, baled straw in California and Illinois, etc. The Imperfect Ditch method of construction is becoming quite commonplace.

Thus, it is seen that the construction procedure described by the authors and its objective of lessening the loads and pressures on culverts under the embankments is not new or of recent origin. However, their analytical treatment of the problem is new and unique, and constitutes a valuable contribution to this area of engineering.

The writer developed a theoretical analysis of imperfect ditch conduit loads prior to 1950 (2), and published an account of its application in 1958 (9). The late W. J. Schlick (10) reported the results of some load-measuring experiments in 1951. An excellent account of the use of baled straw to reduce loads on culverts under high fills in Humboldt County, California, was presented by Norman G. Larsen (11) of the California Division of Highways in 1962.

The writer's theory of loads on this class of buried conduits is based upon the same general principles as the classical Marston theory, i. e., the load on the structure is considered to be equal to the weight of the overlying prism of soil minus the upward shearing forces which are generated along the vertical planes rising from the sides of the imperfect ditch (Fig. 8). The load equation is:

$$W_c = C_n \, w \, B_c^2$$

in which

W_c = load on conduit per unit length;
w = unit weight of fill material;
B_c = outside width of conduit and imperfect ditch;
C_n = a calculation coefficient which is a function of B_c and the height of fill, H; the product, $K\mu$, of the lateral pressure ratio and the coefficient of friction of the fill material; the settlement ratio, r_{sd}; and the projection ratio, p'. Derivations of expressions for C_n are given in Ref. (2).

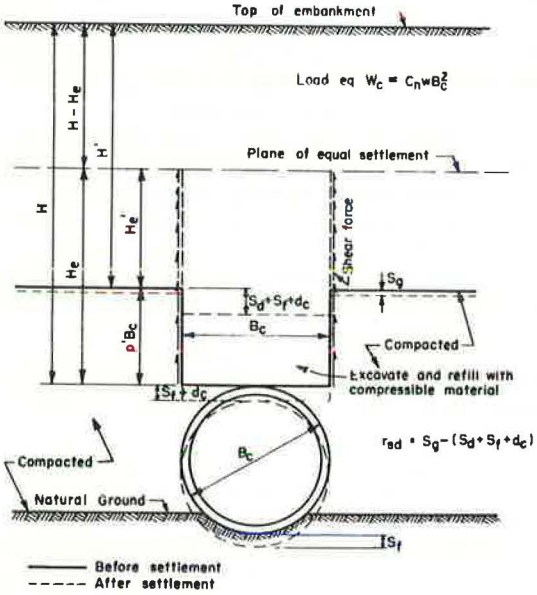

Figure 8. Imperfect ditch construction.

It is of very great interest to calculate the vertical loads on the authors' culvert by the above method and compare the results with those presented in the paper. Considering section 4, the following data apply: H = 233 ft, B_c = 11 ft, w = 120 pcf, p' = 4/11 = 0.36.

The settlement ratio is a rational factor in the development of the load theory. However, it is difficult to evaluate rationally in advance of construction, and the writer has always felt that it should be treated as an empirical factor, usable values of which can best be determined by the observation of the performance of actual structures under load. Present information upon which to base empirical values is very meager. However, the writer has stated (12): "In the absence of factual data relative to probable values of the settlement ratio for conduits of this class, it is tentatively

recommended that this ratio be assumed to lie between -0.3 and -0.5 for the purpose of estimating loads."

Using r_{sd} = -0.5, the estimated vertical load on the culvert at Section 4 is 225,000 lb/lin ft, whereas the pressure at the crown of the culvert (Fig. 3) multiplied by the width 11 ft is approximately 215,000 plf. At Section 2, using r_{sd} = -0.3 the estimated vertical load is 160,000 plf and the reported pressure is 179,000 plf. The agreement between these loads is remarkably close considering the widely divergent methods employed in their computation, and lends credence to both methods of computation.

References

9. Spangler, M. G. A Practical Application of the Imperfect Ditch Method of Construction. HRB Proc., Vol. 37, 1958.
10. Schlick, W. J. Loads on Negative Projecting Conduits. HRB Proc., Vol. 31, 1951.
11. Larsen, Norman G. A Practical Method for Constructing Rigid Conduits Under High Fills. HRB Proc., Vol. 41, 1962.
12. Spangler, M. G. Soil Engineering. 2nd Edition, International Textbook Company, Scranton, Pa., 1960.

S. PAWSEY and C. B. BROWN, Closure—Professor Spangler's considerable addition to the history of the imperfect ditch method puts the effort in this paper into perspective. Naturally no claim of originating the method is made by the authors; however, a rational method of analyzing its effect has been presented. The main departure from Spangler's approach is that the pressure distribution, as opposed to the total force is predicted. With respect to the design of the culvert it is this pressure distribution which is of importance. Only with this knowledge can proper use of structural design procedures be made. In particular, regions with rapid change of pressure and associated high moments and shears can be examined with some confidence. Needless to say, such design activities require knowledge of the actual pressure distribution as opposed to the total vertical force on the culvert. Perhaps of more interest is the possibility of providing fill procedures which insure the most satisfactory pressure distribution from the structural viewpoint.

With regard to Spangler's last paragraph, it is felt that only by the evidence of in situ barrel measurements can the reality of a predicted pressure distribution be defended. References (3, 4) show a measured attenuation of crown pressures on a rigid culvert when a "weak" inclusion was provided. This limited experimental evidence certainly does not vitiate the results presented here, but the authors are sensitive to the necessity for many more data.

Retaining Wall Design—An Example of Small-Scale Optimization

B. B. SCHIMMING, University of Notre Dame, and
J. F. FISCHER, Sverdrup & Parcel and Assoc., Inc., St. Louis

The feasibility of the application of optimization techniques to relatively small civil engineering problems as typified by retaining wall design is presented. The objective function as measured by the cost of concrete and reinforcing steel is minimized with respect to the toe, heel, stem base and footing thickness dimensions.

Four different numerical search techniques are employed in conjunction with a digital computer. They include: an exhaustive search, the converging gradient ascent, the steepest ascent and the random search methods. The relative efficiencies of the various approaches are discussed and compared.

Based on computer running time and programming effort required, it would appear that the state of the art has reached the point where very little additional expenditure is required in order to optimize the design of certain types of relatively small, common civil engineering problems.

•THE advent of the space age has injected a number of particularly meaningful words into the engineering vocabulary. In particular, the words system and optimum are two of the most commonly encountered. Confronted with vast projects composed of many interrelated components (system) involving huge expenditures of capital, the designer found it necessary and justifiable to consider the most efficient (optimum) configuration. The accumulated knowledge from this trend in conjunction with the general availability of digital computers has made it possible to examine the feasibility of applying optimal design to smaller systems.

If a physical system exhibits a structure which can be represented by a mathematical model, and if the value or merit of the system can be quantified as a function of the design variables, then some algorithm may be evolved for choosing the "best" answer. This procedure is generally referred to as mathematical programming.

The general programming problem seeks to minimize or maximize an objective function for n variables:

$$z = f(x_j);\ j = 1, \ldots n$$

subject to m inequality or equality constraints,

$$g_i(x_j) \geq = \leq b_i;\ i = 1, \ldots m$$
$$j = 1, \ldots n$$

with feasible solutions

$$x_j \geq 0 \qquad j = 1, \ldots n$$

In other words, the vector of independent variable values which yields the largest or smallest value of the objective function is sought within the region bounded by constraints.

Paper sponsored by Committee on Mechanics of Earth Masses and Layered Systems and presented at the 47th Annual Meeting.

As in most areas of analysis, the first successful approach to the general programming problem involved the linear case which can be stated as follows: $f(x_j)$ is a linear combination of the variables x_j and each $g_i(x_j)$ is also a linear transformation. The algorithm, referred to as the simplex method, for solving the linear programming problem was first introduced by G. B. Dantzig (1) in 1948.

The second important class of programming problems falls under the heading of nonlinear programming. In this case $f(x_j)$ or at least one $g_i(x_j)$ is nonlinear in at least one x_j. The nonlinearity, as might be suspected, considerably increases the difficulty of obtaining a solution. A number of relatively formal methods have been proposed to solve the nonlinear case (2, 3, 4).

Often it may be necessary to resort to a numerical approximation when confronted with a nonlinear programming problem. Conceptually, the numerical approach is usually easier, yet computationally more demanding.

In order to examine the present feasibility of relatively small design optimization, three different numerical approaches were applied to a typical nonlinear civil engineering design problem—retaining wall design. The normal design of retaining walls using a digital computer has been previously discussed by Wadsworth (5).

PROBLEM DEFINITION

The type of retaining wall chosen for analysis is shown in Figure 1. It is basically a cantilever wall with no key. The height of the wall (H) above subgrade, including the required depth (D) to avoid frost action, and the thickness of the stem at the top (TT) are given dimensions, along with the slope of the soil behind the wall and the necessary soil properties. The remaining four dimensions are taken as the design variables:

TB = thickness of stem at bottom,
TOE = toe length,
HEEL = heel length, and
B = base thickness.

There are many constraints which a cantilever retaining wall must satisfy, the first one being stability. Both overturning and sliding stability must be considered, with a minimum allowable factor of safety specified. The stability constraints used are those presented by Peck, Hanson and Thornburn (6) for a 1-ft length of wall. The remaining constraints are all of the requirements dictated by the American Concrete Institute Building Code Requirements for Reinforced Concrete - ACI 318-637.

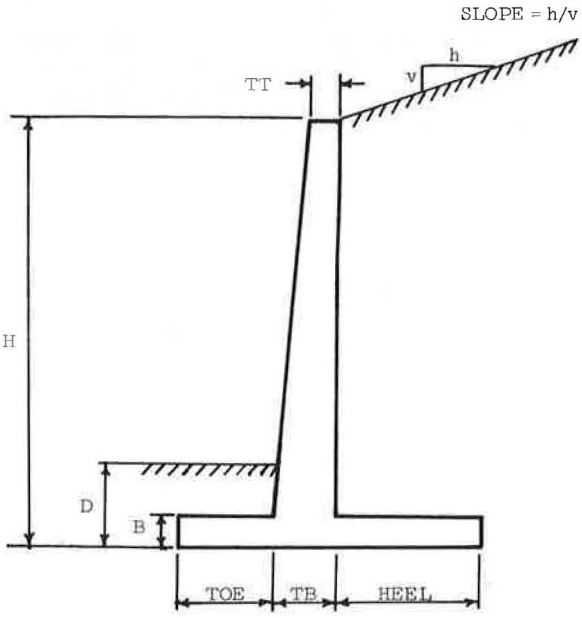

Figure 1. Cantilever retaining wall, no key.

The objective function measures the volume of concrete and the weight of reinforcing steel per lineal foot of wall and multiplies these values by their respective unit costs. The unit cost of ready-mix concrete and reinforcing steel are those for St. Louis, Missouri, obtained from a recent issue of Engineering News-Record (8).

Examination of the constraints and the objective function indicates that the retaining wall problem is nonlinear. For example, the cross sectional area of the footing involves products of the design variable thus resulting in a nonlinear combination. In addition, the objective function is not explicitly

TABLE 1

INPUT DATA

Definition	Symbol	Value
Stem thickness at top, in.	TT	12.000
Total height, ft	H	16.500
Slope of soil surface behind wall	Slope	3.000
Soil depth in front of wall, ft	D	3.500
K-sub-V, ksf, (k_v)	VK	0.009
K-sub-H, ksf, (k_h)	HK	0.033
Unit weight of soil, kcf	GS	0.125
Unit weight of concrete, kcf	GC	0.150
Allowable soil pressure, ksf	QA	3.000
Friction between soil and base, ksf	SF	0.550
Overturning factor of safety	OFS	1.500
Sliding factor of safety	SFS	1.500
Compressive strength of concrete, psi	FC	3750.0
Allowable steel tensile stress, ksi	FS	24.000
Allowable concrete shear stress, psi	FSH	67.000
Modular ratio N, E(steel)/E(concrete)	EN	8.250
Balanced design J	FJ	0.8781
Balanced design R, psi	ARE	271.00
Unit price of re-bars, $/100 lb	US	9.850
Unit price of ready-mix, $/cu yd	UC	13.500

Bar Size	Bar Diameter (in.)	Bar Area (sq in)	Bar Perimeter (in.)	Bar Weight (lb/ft)
3	0.375	0.11	1.178	0.376
4	0.500	0.20	1.571	0.668
5	0.625	0.31	1.963	1.043
6	0.750	0.44	2.356	1.502
7	0.875	0.60	2.749	2.044
8	1.000	0.79	3.142	2.670
9	1.128	1.00	3.544	3.400
10	1.270	1.27	3.990	4.303
11	1.410	1.56	4.430	5.313

expressed in terms of the design variables. These conditions strongly suggest the use of numerical optimization techniques.

The input data, design variables, constraints and objective function information are summarized in Tables 1 through 3. The actual wall to be optimized was again chosen from Peck, Hanson and Thornburn thus providing the input data. The concrete and steel specifications in the problem were replaced by the most recent reinforced concrete code and the reinforcing steel properties were those of standard deformed bars (ASMT A15, A305).

METHODOLOGY

Essentially, three different search techniques were pursued for the purpose of comparing their relative efficiency for this type of application. In addition, an exhaustive search which examined all possible outcomes was conducted as a reference base.

A brief introduction to the three search methods is presented for explanatory purposes; however, the interested reader should consult a reference such as Wilde (9) to become aware of the pitfalls and limitations of each of the approaches.

The response surface is a plot of the objective function versus the independent variables. For the retaining wall problem the response surface would be a 5-dimensional plot of cost versus the 4 variable distances. The criterion for the existence of a maximum or minimum in an n + 1 dimensional space is that the gradient

TABLE 2

VARIABLES: RANGES AND INCREMENTS

Variable	Integer Associated With Variable	Increment Size for Variable	Range of Variable	Corresponding Range of Associated Integer	Number of Increments
TB	ITB	1.00"	13"-30"	1-18	18
TOE	ITOE	0.25'	0.25'-8.00'	1-32	32
HEEL	IHEEL	0.50'	0.50'-16.00'	1-32	32
B	IB	0.25'	0.25'-3.00'	1-12	12

Note: The number of possible combinations of the variables: 18 x 32 x 32 x 12 = 221, 184

In general: TB (in.) = ITB x 1.00 + TT
TOE (ft) = ITOE x 0.25
HEEL (ft) = IHEEL x 0.50
B (ft) = IB x 0.25

TABLE 3

CONSTRAINTS AND OBJECTIVE FUNCTION

Stability Constraints	
Eccentricity of resultant soil reaction between center of base and toe, and also within kern	$0 \leq E \leq BASE/6$
Soil pressure at toe non-negative and less than or equal to allowable	$0 \leq QTOE \leq QA$
Soil pressure at heel non-negative and less than or equal to allowable	$0 \leq QHEEL \leq QA$
Overturning factor of safety not less than minimum allowable	$AOFS \geq OFS$
Sliding factor of safety not less than minimum allowable	$SFSMIN \geq SFS$
Concrete and Re-Bar Design Constraints	
Effective depth not less than that required for shear	$DA \geq DS$
Effective depth not less than that required for moment	$DA \geq DM$
Clear space between re-bars not less than one inch	$CSPACE \geq 1$
Clear space between re-bars not less than bar diameter	$CSPACE \geq BARD$
Center-to-center spacing of re-bars not greater than three times the total concrete thickness	$SPACE \leq T3$
Center-to-center spacing of re-bars not greater than 18 in.	$SPACE \leq 18$
Actual bond stress not greater than allowable	$BOND \leq ABOND$
Objective Function	
Minimize combined total cost of concrete and steel per lineal foot of cantilever retaining wall:	
COST = Total volume of concrete per foot (cu yd) times unit cost of concrete ($/cu yd); plus total weight of steel per foot (100 lb), times unit cost of steel ($/100 lb).	

$$\nabla f(\underline{x}) = \begin{bmatrix} \frac{\partial f}{\partial x_1} \\ \frac{\partial f}{\partial x_2} \\ \cdot \\ \cdot \\ \frac{\partial f}{\partial x_n} \end{bmatrix} = 0$$

Since the gradient is a vector quantity, it has both magnitude and direction. Its magnitude corresponds to the value of the "slope" of the response surface and its direction to the direction of the "steepest slope." Therefore, knowing the gradient at a point indicates the most efficient manner to proceed toward a "peak."

The gradient concept is at the heart of the "steepest ascent" technique. An initial point is chosen, the gradient calculated and a "step" is taken in the direction of the gradient. The process is repeated until a zero gradient is obtained which locates the optimum value of the response surface, if there is only one peak present in the region of interest.

For the retaining wall problem the gradient cannot be determined by partial differentiation because of the implicit nature of the objective function. Thus experiments were performed by evaluating the objective function in the neighborhood to determine the direction of steepest descent. For the 5-dimensional space, $5^4 = 625$, local experiments were performed at each intermediate point. Any point that was encountered which violated a constraint was simply assigned a large positive number to eliminate it from further consideration.

The converging gradient ascent technique embodies a similar philosophy except that each independent variable is searched sequentially while the remaining independent variables are fixed at their previously evaluated minimums.

The random search procedure as proposed by Brooks (10) has two attractive features which are pointed out by Wilde (9). First, no assumption about the form of the response surface need be made. Second, the probability p(f) of finding at least one solution in the best fraction f of the experimental region does not depend on the number of dimensions, for after n trials have been made at random,

or

$$p(f) = 1 - (1 - f)^n$$

$$n = \frac{\log [\, 1 - p(f)]}{\log (1 - f)}$$

TABLE 4

NUMBER OF TRIALS n REQUIRED IN AN OPTIMUM-SEEKING EXPERIMENT CONDUCTED BY THE RANDOM METHOD, IN ORDER TO BE IN THE BEST FRACTION f WITH PROBABILITY p(f)

f	p(f)				
	0.80	0.90	0.95	0.99	0.999
0.10	16	22	29	44	66
0.05	32	45	59	90	135
0.025	64	91	119	182	273
0.01	161	230	299	459	688
0.005	322	460	598	919	1379
0.001	1609	2302	2995	4603	6905

Reference (9).

The effectiveness of this relation is portrayed in Table 4. To apply the random search method, a value for a variable within its allowable range is chosen randomly with a "random number generator" subroutine. A different random number is selected for each independent variable in this manner and then the objective function is evaluated for the trial combination. After any number of trial solutions, the best combination of the independent variables found up to that point is known along with the current optimum value of the objective function. Thus after n trials, the current optimum has a probability p(f) of being within the best fraction f of all possible outcomes.

It should be noted that the simplest form of random search has been employed in this study. Significant efficiencies may be required as the dimensions of the problem increase. Socalled imbedding procedures (11) and the use of concepts from the area of statistical design of experiments (12) can be a worthwhile aid in this quest for efficiency.

RESULTS

The results of the exhaustive search for the wall presented in Table 1 are summarized in Table 5. For the range of design variables chosen, only 12 percent of the possible walls did not violate the constraints. Examination of the ranges indicates an overextension thus including obviously inappropriate cases. However, the other extreme of too narrow a range based on intuition may in fact yield a sub-optimum answer.

TABLE 5

RESULTS OF EXHAUSTIVE SEARCH

For Data of Table 1, 1963 Specifications	
The optimum cost per lineal foot of wall is	$17.28
Determined in 221184 trials	
with 26048 walls satisfactory	
Optimum dimensions are TB = 1.1667 ft	B = 1.000 ft
TOE = 3.2500 ft	HEEL = 4.000 ft
Eccentricity E of resultant soil reaction is	0.74 ft
Soil pressure at TOE QTOE is	2.60≤3.00 ksf ...OK
Soil pressure at HEEL QHEEL is	0.81≤3.00 ksf ...OK
Overturning factor of safety is	2.59≥1.50.....OK
Sliding factor of safety is	1.50≥1.50.....OK
Stem results	
Number 5 bars, at 3.50 in. center to center	
Cut off half of bars 5.32 ft from bottom of stem	
Cut off ¼ of bars 8.50 ft from bottom of stem	
Toe results	
Number 7 bars, at 10.00 in. center to center	
Heel results	
Number 8 bars, at 15.00 in. center to center	

TABLE 6

Search Technique	Converging Gradient Ascent	Steepest Ascent
Number of trials	224	1875
Number of successful trials	138	883
Computer run time	45 sec	2 min 10 sec
Minimum cost	$17.28	$17.28

Peck, Hanson and Thornburn state that for best results, trial dimensions should be within the following proportions:

BASE/H	= 0.40 to 0.65
TOE/BASE	= approx. $\frac{1}{3}$
B/H	= $\frac{1}{12}$ to $\frac{1}{8}$
Stem taper	= $\frac{1}{4}$ to $\frac{3}{4}$ in./ft

The optimum wall ratios are:

BASE/H	= 0.51
TOE/BASE	= 0.39
B/H	= approx. $\frac{1}{16}$
Stem taper	= approx. $\frac{1}{8}$ in./ft

These results seem to indicate that the trial ratios might be revised using current specifications. However, caution should be exercised in view of the dependence of the result

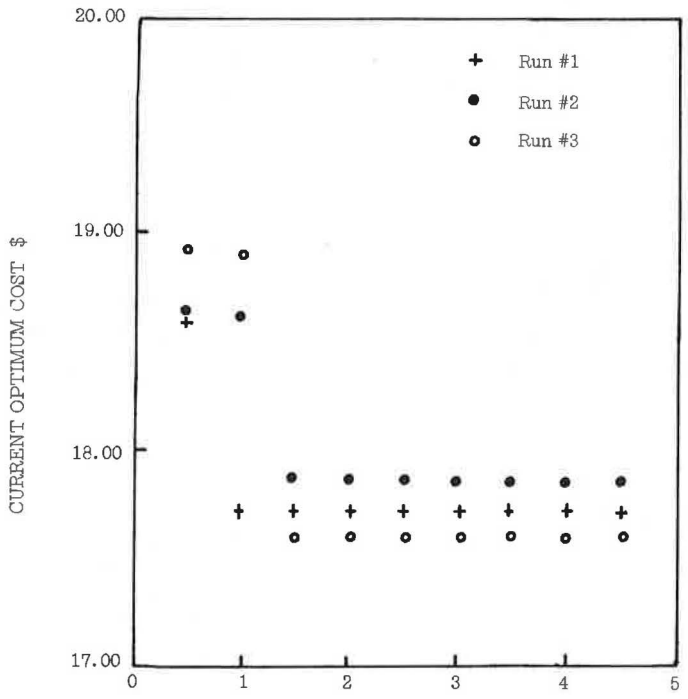

Figure 2. Random search results.

on the unit costs of the materials. The computer run time on a UNIVAC 1107 at the University of Notre Dame where the authors conducted the study for the exhaustive search was 25 min and 17 sec.

The results of the converging gradient ascent and steepest ascent search are compared in Table 6.

It should be remembered when examining these results that the relative efficiency is quite dependent on the proximity of the starting point to the optimum. In addition, the rapid convergence of the geometric techniques is quite dependent on the nature of the objective function being examined.

The results of three successive runs of 5000 trials each, using the random search approach are shown in Figure 2. All three runs yielded a solution with a cost within 5 percent of the optimum cost after 2000 trials. It should be noted that proximity to the optimum based on cost is not synonymous with the best fraction f in Table 4 because of the nonlinear distribution of number of walls in a particular price bracket. Based on a computation rate of approximately 800 trials per minute, the 2000 trial search was accomplished in approximately $2\frac{1}{2}$ minutes. It is true that the unique optimum was not obtained in this case; however, the ease of application and flexibility tend to balance the limitations.

CONCLUSIONS

In any optimization problem, the designer must balance the following factors:

1. Anticipated savings in construction costs resulting from an optimization over a conventional design;
2. Cost of computer running time; and
3. Cost of formulating the optimizing algorithm which is of course related to its sophistication.

With regard to the retaining wall example, it has been shown that all three optimization techniques involved computer running times of $\frac{1}{20}$ hr or less. At existing computer rates this becomes almost a trivial amount.

The cost of formulating and perfecting the computer program is less easily quantified. It is a function of the complexity of the technique and the talent of the programmer. The search techniques employed in this investigation are quite general and yet do not require any undue mathematical prowess. Also, the burden of program formulation will probably be considerably eased in the near future as general purpose optimization programs become available.

The economy of construction costs must of course be judged on an individual basis; however, in view of the previous discussion the benefits of optimization would not have to be large to justify the effort.

At the risk of possibly stating the obvious, there would appear to be a class of relatively small, common civil engineering design problems that can be optimized on an economically justifiable basis in a relatively straightforward manner in conjunction with digital computation.

REFERENCES

1. Dantzig, G. B. Programming in a Linear Structure. Comptroller, USAF, Washington, D.C., Feb. 1948.
2. Hadley, G. Nonlinear and Dynamic Programming. Addison-Wesley, 1964.
3. Kuhn, H.W., and Tucker, A. W. Nonlinear Programming. Proceedings of the Second Berkeley Symposium on Mathematical Statistics and Probability, Berkeley, University of California Press, pp. 481-492, 1950.
4. Arrow, K. J., Hurwicz, L., and Uzawa, H. Studies in Linear and Non Linear Programming. Stanford University Press, 1958.
5. Wadsworth, M. A. Sloping Surcharge Retaining Wall Design. 2nd. ASCE Conference on Electronic Computation, Sept. 1960.
6. Peck, R. B., Hanson, W. E., and Thornburn, H. Foundation Engineering. John Wiley & Sons, Inc., 1953.

7. Building Code Requirements for Reinforced Concrete (ACI 318-63). Detroit: American Concrete Institute, 1963.
8. Materials Prices—Monthly Market Quotation by ENR Field Reporters. Engineering News-Record, Vol. 178, No. 1, p. 46, Jan. 5, 1967; Vol. 178, No. 2, p. 54, Jan. 12, 1967.
9. Wilde, D. J., Optimum Searching Methods. Prentice Hall, Inc., 1964.
10. Brooks, S. H. A Discussion of Random Methods for Maximum. Operations Research, Vol. 6., No. 2, p. 244-251., March 1958.
11. Mathematical Optimization Techniques. Computers in Engineering Design Education. University of Michigan, Vol. 1, p. 42-82, 1966.
12. Hicks, C. R., Fundamental Concepts in the Design of Experiments. Holt, Rinehart and Winston, 1964.

Discussion

G. G. GOBLE, Associate Professor, Case Western Reserve University—This paper gives an interesting application of mathematical programming in civil engineering design. Since a substantial amount of work has been done in applying these methods in structural design, a listing of a few references may be useful to the reader. References (13) through (16) discuss the practical application of optimization in structural design. In references, (17)and (18) the use of linear programming is discussed. Nonlinear programming has been applied in references (19), (20) and (21) while in reference (22), the structural design problem is converted into an unconstrained minimization problem. This very brief list is by no means complete, but provides a review of the development of the field. In some of the references highly developed search techniques were used.

The writer agrees enthusiastically with the conclusion that optimizing techniques are ready for routine application in civil engineering design. Perhaps, the greatest impact will come from the freeing of the designer from many tedious design computations so that his effort can be spent on more creative tasks.

References

13. Razani, R., and Goble, G. Optimum Design of Constant Depth Plate Girders. Jour. of Struct. Div. ASCE, Vol. 92, No. ST2, April 1966.
14. Goble, G., and DeSantis, P. Optimum Design of Composite Girders with Mixed Steel Strengths. Jour. of Struct. Div. ASCE, Vol. 92, No. ST6, April 1966.
15. Goble, G. Structural Synthesis in Cost Oriented Structural Design. Building Research, March-April 1966.
16. Brown, D. and Ang, A. Structural Optimization by Nonlinear Programming. Jour. of Struct. Div. ASCE, Vol. 92, No. ST6, Dec. 1966.
17. Reinschmidt, K., Cornell, C., and Brotchie, J. Iterative Design and Structural Optimization. Jour. of Struct. Div. ASCE, Vol. 92, No. ST6, Dec. 1966.
18. Moses, F. Optimum Structural Design Using Linear Programming. Jour. of Struct. Div. ASCE, Vol. 90, No. ST6, Dec. 1964.
19. Schmit, L A. Structural Design by Systematic Synthesis. Proc. 2nd National Conference on Electronic Computation, Struct. Div. ASCE, Sept. 1960.
20. Schmit, L. A., and Kicher, T. P. Synthesis of Material and Configuration Selection. Jour. of Struct. Div. ASCE, Vol. 88, No. ST3, June 1962.
21 Schmit, L. A., and Mallett, R. H. Structural Synthesis and the Design Parameter Hierarchy. Jour. Struct. Div. ASCE, Vol. 89, No. ST4, Aug. 1963.
22. Schmit, L. A., and Fox, R. L. An Integrated Approach to Structural Synthesis and Analysis. AIAA Jour. Vol. 3, No 6, June 1965.